REPORT DOCUMENTATION PAGE

Form Approved OMB No. 0704-0188

1. REPORT DATE *(DD-MM-YYYY)*	2. REPORT TYPE	3. DATES COVERED *(From – To)*
08-02-2008	Final Report	1 February 2007 - 01-Feb-08

4. TITLE AND SUBTITLE

Interaction of Semiconductor Obstacle with Electromagnetic Wave Propagating in Circular Waveguide

5a. CONTRACT NUMBER
FA8655-07-1-3028

5b. GRANT NUMBER

5c. PROGRAM ELEMENT NUMBER

6. AUTHOR(S)

Dr. Zilvinas Kancleris

5d. PROJECT NUMBER

5d. TASK NUMBER

5e. WORK UNIT NUMBER

7. PERFORMING ORGANIZATION NAME(S) AND ADDRESS(ES)

Semiconductor Physics Institute
Microwave Laboratory
A. Gostauto 11
Vilnius LT-01108
Lithuania

8. PERFORMING ORGANIZATION REPORT NUMBER

N/A

9. SPONSORING/MONITORING AGENCY NAME(S) AND ADDRESS(ES)

EOARD
Unit 4515 BOX 14
APO AE 09421

10. SPONSOR/MONITOR'S ACRONYM(S)

11. SPONSOR/MONITOR'S REPORT NUMBER(S)
Grant 07-3028

12. DISTRIBUTION/AVAILABILITY STATEMENT

Approved for public release; distribution is unlimited.

13. SUPPLEMENTARY NOTES

14. ABSTRACT

This report results from a contract tasking Semiconductor Physics Institute as follows: To achieve the proposed goals, the modeling of the circular waveguide section containing semiconductor obstacle will be performed. To calculate the average electric field in the semiconductor obstacle the finite difference time domain method will be used. Although, the lowest critical frequency in the circular waveguide is characteristic to H11 mode higher modes such as E01 and H01 are also sometimes used. Depending on mode some components of electromagnetic field are suppressed, nevertheless in the vicinity of the obstacle all six components of electromagnetic field might be excited and they should be taken into account when determining averaged electric field in the semiconductor obstacle. Since the resistive sensor actually feels the amplitude of electric field, the distribution of electric field component within the waveguide should have a crucial influence on the performance of the sensor and this fact should be taken into account in sensors design. Therefore it is also planning to investigate the behavior of the averaged electric field in the semiconductor obstacle when different modes are excited in the waveguide.
To perform investigation it is planned to use internal programs for the modeling of electromagnetic wave propagating in the circular waveguide with the obstacle. Such modeling has already been done in rectangular waveguide with semiconductor obstacle placed on a wide wall of the waveguide and in the obstacle under the thin metal diaphragm. In both cases all six components of electromagnetic field in Cartesian coordinate system has been determined. It is planned to modify the program so that it should be able to calculate the electromagnetic field components in cylindrical coordinate system.

15. SUBJECT TERMS
EOARD, Detector Technology, Microwave Technology

16. SECURITY CLASSIFICATION OF:			17. LIMITATION OF ABSTRACT	18, NUMBER OF PAGES	19a. NAME OF RESPONSIBLE PERSON
a. REPORT	b. ABSTRACT	c. THIS PAGE			A. GAVRIELIDES
UNCLAS	UNCLAS	UNCLAS	UL	32	19b. TELEPHONE NUMBER *(Include area code)* +44 (0)1895 616205

INTERACTION OF SEMICONDUCTOR OBSTACLE WITH ELECTROMAGNETIC WAVE PROPAGATING IN CIRCULAR WAVEGUIDE

(Final report)

Microwave Laboratory, Semiconductor Physics Institute
A. Goštauto 11, Vilnius LT 01108, Lithuania
tel.: 370 5 261 9808
fax.: 370 5 262 7123
e-mail: kancleris@uj.pfi.lt

Vilnius, 2008

Contents

Microwave Laboratory of Semiconductor Physics Institute has performed this work under the contract FA8655-07-1-3028 issued by European Office of Aerospace Research and Development (EOARD).
Principal investigator: Žilvinas Kancleris, Dr. Habil., Head of Microwave Laboratory.

1 Introduction

At present, different types of pulsed high power microwave (HPM) oscillators and amplifiers are being researched in laboratories, as well as being manufactured by industry. They are used in communication systems, radars, electromagnetic testing facilities, scientific research, and military projects. In the experiments with relativistic electron beams, a circular waveguide with a horn antenna is often used providing radiation of generated pulse from the HPM facility into free space. Systems measuring generated power are usually located at some distance from the radiating antenna. They consist of the receiving antenna connected to the device enabling the measurement of microwave pulses.

To-date the main device being used for the measurement of the HPM pulse power is a semiconductor diode. It is able to measure microwave pulse power up to a few hundreds of mW [1]. Therefore, when it is used to measure HPM pulses, the initial pulse has to be strongly attenuated. On the one hand, large attenuation of the microwave pulse results in the decrease of the measurement accuracy. In addition, the size and weight of the measurement system increases, and its control becomes complicated. On the other hand, when the measured pulsed microwave power is of the order of mW, the diode outputs a DC pulse with amplitude of the order of mV. To measure so small DC signal in the presence of the stray pick-up and electromagnetic interference that are typical in the environment of HPM sources, a shielded chamber with a measurement equipment situated at a respectful distance from the HPM source is usually employed. The installation of the shielded chamber confines the flexibility of the measurement system and increases its price.

In Microwave Laboratory of Semiconductor Physics Institute, we have developed an alternative device for the HPM pulse measurement – a resistive sensor (RS), performance of which is based on the electron heating effect in semiconductors. A sensing element (SE) of the RS is inserted into transmission line – usually the rectangular waveguide. The electric field of the microwave pulse traveling in the waveguide heats electrons in the SE its resistance increases and by measuring this resistance change the microwave pulse power in the transmission line is determined. The main advantages of the RS over the diode are the following: it can measure HPM pulses directly, produces high output signal, is overload resistant, and demonstrates very good long term stability [2]. The resistive sensors developed in our laboratory for rectangular waveguides are used in laboratories dealing with HPM pulses worldwide. Unfortunately, the RS for the circular waveguide has not been designed yet.

Having in mind the drawback of the measurement of HPM pulses in facilities employing circular waveguides in the output, our activities under the current project will be concentrated on the elucidation of peculiarities of the interaction of the electromagnetic wave propagating in the circular waveguide with a semiconductor obstacle placed on the waveguide wall. Our task is to find such parameters of the obstacle that it can serve as the prototype of the SE for the circular waveguide RS. Considering the semiconductor obstacle from this point of view, the main requirements for it can be formulated. First, the SE should not insert considerable reflection in the waveguide, so the value of VSWR has been set at < 1.2. Second, the RS should be able to measure nanosecond-duration HPM pulses; therefore, the DC resistance of the RS should not exceed 50 Ω. Third, the shape of the SE should be taken as a plate that is important for heat transfer from the SE. Finally, the flat frequency response of the RS in the waveguide's frequency band is preferable.

In the interim report [3], the investigations of the interaction of the semiconductor obstacle with (TE_{01}) H_{01} mode electromagnetic wave propagating in the circular waveguide were presented. In the final report, we have considered (TE_{11}) H_{11} mode that is the lowest mode propagating in the circular waveguide. The final report is organized as follows. In

Section 2 main features of the H_{11} mode in the circular waveguide are recalled. The layout of the SE in the circular waveguide, the output signal and the sensitivity of the RS are considered in Section 3. A finite difference time domain (FDTD) method and programs used for electromagnetic field components calculation in the cylindrical coordinate system are briefly presented in Section 4. Modeling results for two different configurations of the SE are described in Section 5 and Section 6, respectively. In Appendix, the test results of the program for H_{11} mode are presented.

2 H_{11} mode in a circular waveguide

Features of the H_{11} mode in the circular waveguide are summarized in this section. Electromagnetic field components as well as the power transmitted through the waveguide are considered.

2.1 Electromagnetic field components

Although the H_{01} mode, which has been considered in the interim report [3], is the simplest TE mode in a circular waveguide, it is not the lowest one. This illustrates the data presented in Fig. 1, where critical wavelengths and frequencies for different modes in a waveguide with radius a = 1 cm are shown. As one can see from the figure, the critical frequency of the H_{11} mode is the lowest. The regular H_{11} wave has five components: E_φ, E_r, H_φ, H_r and H_z. As one can see from Fig. 2, the components are dependent on the azimuthal angle φ. Plane A–A, where the electric field has E_r component only, sometimes is called a polarization plane.

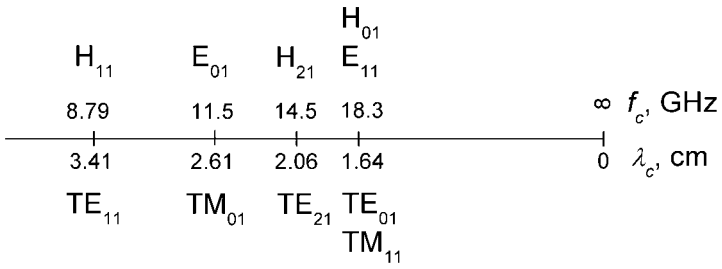

Fig. 1. Critical frequencies and wavelengths for different modes in a circular waveguide.

Dependences of the amplitudes of the regular wave on the radial r and azimuthal φ

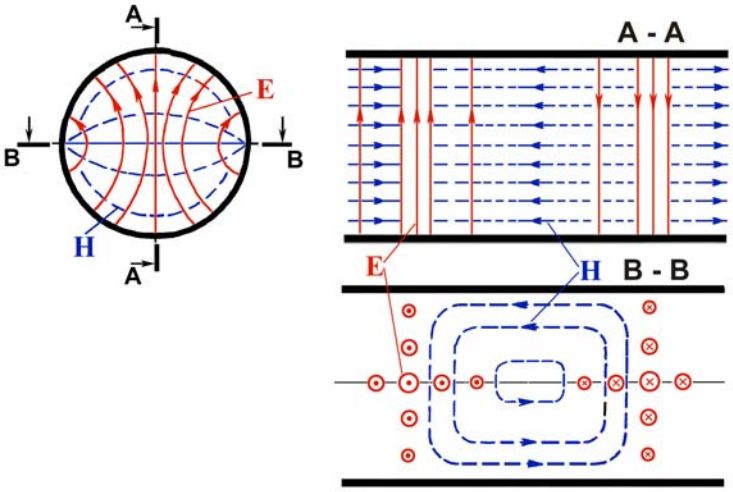

Fig. 2. The view of lines of the electromagnetic field in the circular waveguide for mode H_{11}.

coordinates can be expressed in the following way [4]

$$E_r(r,\varphi) = Aa\frac{J_1(\mu_{11}r/a)}{\mu_{11}r}\cos\varphi, \tag{1}$$

$$E_\varphi(r,\varphi) = -AJ_1^{'}(\mu_{11}r/a)\sin\varphi, \tag{2}$$

$$H_r(r,z) = -A\frac{\lambda}{\lambda_w}\sqrt{\frac{\varepsilon_0}{\mu_0}}J_1^{'}(\mu_{11}r/a)\sin\varphi, \tag{3}$$

$$H_\varphi(r,z) = Aa\frac{\lambda}{\lambda_c}\sqrt{\frac{\varepsilon_0}{\mu_0}}\frac{J_1(\mu_{11}r/a)}{\mu_{11}r}\cos\varphi. \tag{4}$$

$$H_z(r,z) = A\frac{\lambda}{\lambda_c}\sqrt{\frac{\varepsilon_0}{\mu_0}}J_1(\mu_{11}r/a)\sin\varphi. \tag{5}$$

Here the coefficient A is measured in electric field units and it depends on the power propagating through the waveguide, λ, λ_w, and λ_c are the wavelength of electromagnetic oscillations in free space, in a waveguide, and the critical wavelength for the H_{11} mode, respectively, ε_0 and μ_0 are the vacuum permittivity and permeability, J_1 and $J_1^{'}$ are the first kind and first order Bessel function and its derivative, μ_{11}=1.8412 is the root of $J_1^{'}$: $J_1^{'}(\mu_{11}) = 0$, and a is a radius of the waveguide. The shape of the Bessel functions appearing in (1)-(5) expressions is shown in Fig. 3. It is seen that the maximum of radial and azimuthal components of the electromagnetic field is reached in the center of the waveguide while the axial component of the magnetic field gets its maximum at a metal wall of the circular waveguide. The following expression describes the critical wavelength for the H_{11} mode [4]

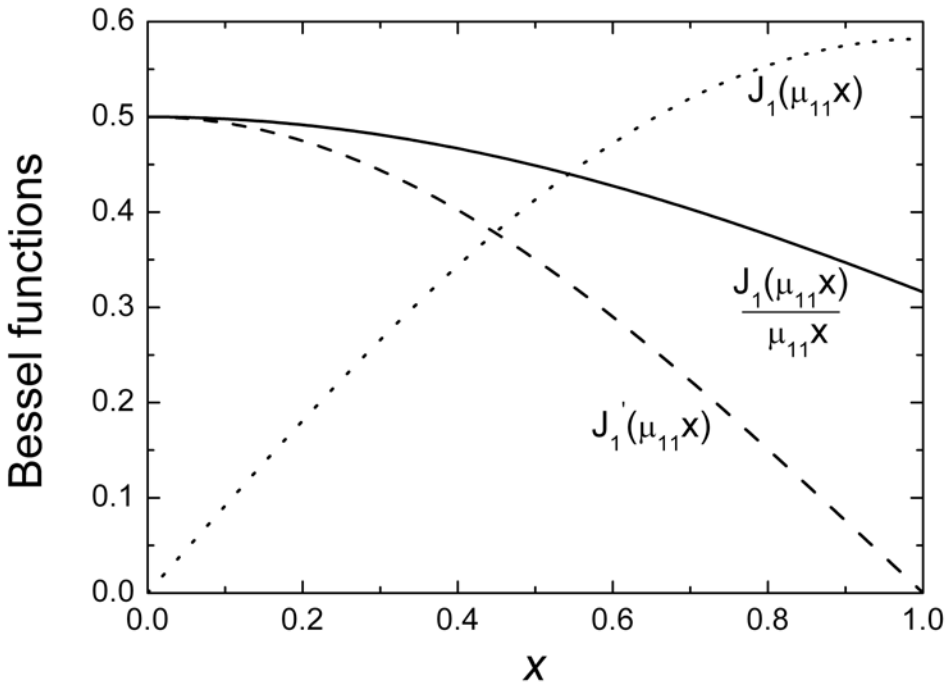

Fig. 3. The shape of Bessel functions appearing in (1)-(5).

$$\lambda_c = \frac{2\pi a}{\mu_{11}} = 3.4125a\,, \tag{6}$$

and the wavelength in the waveguide is expressed in a usual way

$$\lambda_w = \frac{\lambda}{\sqrt{1-\left(\lambda/\lambda_c\right)^2}}\,. \tag{7}$$

2.2 Power

The power transfer by the H_{11} mode can by straightforwardly computed by integrating the Pointing vector over cross sectional area of the waveguide. Making use of (1)-(4) one can get the following expression describing power transmitted through the waveguide for the H_{11} mode

$$P = \frac{\pi\lambda a^2 A^2}{2\lambda_w \mu_{11}^2}\sqrt{\frac{\varepsilon_0}{\mu_0}}\left[\int_0^{\mu_{11}}\left(\frac{J_1(x)}{x}\right)^2 x\,dx + \int_0^{\mu_{11}}\left(J_1'(x)\right)^2 x\,dx\right]. \tag{8}$$

The coefficient A can be related to the maximum electric field amplitude in the regular H_{11} wave in the center of the waveguide. From (1) and (2) follows

$$A = 2E_0\,, \tag{9}$$

where E_0 is the maximum electric field strength of the components E_φ and E_r in the center of the waveguide. Inserting (7) and (9) into (8) and performing integration one can get the following expression

$$P = \pi\frac{\sqrt{1-\left(\lambda/\lambda_c\right)^2}}{\sqrt{\mu_0/\varepsilon_0}}\left[J_0^2(\mu_{11}) + \left(1-\frac{2}{\mu_{11}^2}\right)J_1^2(\mu_{11})\right]a^2E_0^2\,, \tag{10}$$

describing power transmitted through the waveguide. Bessel function values are $J_0(\mu_{11})$=0.3160 and $J_1(\mu_{11})$=0.5819. From (10), the maximum electric field strength in the waveguide at a given power transmitted through the waveguide can be also determined.

3 Resistive sensor in circular waveguide

In this section, the RS in a circular waveguide is considered. Since the possible layouts of the SE are discussed in detail in the interim report [3] in the first subsection we present only brief description of the layout of the plate with metal contacts used in the calculations. The output signal and sensitivity of the RS are considered in the following two subsections.

3.1 Layout of the sensing element

As it was already mentioned in the Introduction, the performance of the RS is based on the electron heating effect in semiconductors. Thus, the SE is actually a resistor made from n-type Si with two ohmic contacts. Therefore, any plate inserted in the waveguide with properly arranged contacts could serve as the SE. The cross sectional view of such a plate in a circular waveguide and its characteristic transverse dimensions are shown in Fig. 4. The length of the plate in the wave propagation direction is denoted as *l*. Depending on the position of the metal contact on the plate, two configurations showed in Fig. 4 have been proposed. A plate with the contacts on its top and bottom was named as a “vertical” configuration (Fig. 4a), while a plate with the contacts on sidewalls of the plate got a name “horizontal” (Fig. 4b). These two names will be used further without quotes to denote the particular configuration of the SE. The possible practical realization of both configurations was considered in the interim report [3].

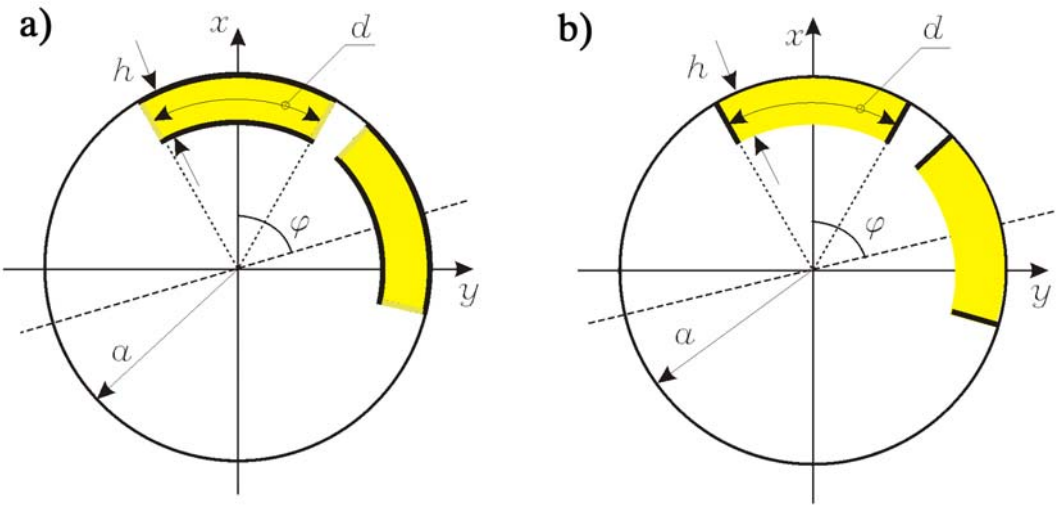

Fig. 4. A plate of the semiconductor with metal contacts on the wall of the circular waveguide: a) contacts on top and bottom surfaces – "vertical" configuration, b) contacts on the sidewalls – "horizontal" configuration.

It should be noted that the amplitudes of electric field of the regular wave depends on azimuthal angle φ (ref. to (1) and (2)). At $\varphi = 0°$ the component E_r gets maximum (1) while at $\varphi = 90$ – E_φ. Since the average electric field in the SE might be dependent on the angle between obstacle and polarization plane, the calculations should be performed for the SE situated at different angles φ in respect to the polarization plane, as it is shown in Fig. 4.

3.2 Output signal

An output signal from the RS being measured using a high input resistance measuring unit can be expressed in the following way

$$U_S = U_0 \frac{\Delta R}{R}, \tag{11}$$

where U_0 is a DC voltage drop on the sensor and $\Delta R/R$ is a relative resistance change of the SE in the microwave electric field. It is well established that in the limit of the slightly heating electric field the relative resistance change is proportional to the square of the electric field [2]

$$\frac{\Delta R}{R} = \beta^* \langle E \rangle^2 \tag{12}$$

where β^* is so-called an effective warm-electron coefficient and $\langle E \rangle$ is an average amplitude of the electric field in the SE. The region, where expression (12) is valid, is called a warm-electron region. In general, the effective warm electron coefficient is frequency dependent and it decreases while the frequency increases. In the present investigation we do not take into account this effect therefore our findings can be used up to and including X-band where the decrease of β^* with frequency is less than 3%.

Experimental investigations have revealed that the warm-electron approximation holds well up to electric field roughly 1 kV/cm where $\Delta R/R$ is of the order of 10%. At a higher electric field, there is considerable deviation of the relative resistance change from the dependence predicted by expression (12). It was found that over a wider range of the electric field strength, the resistance change is described by the following empirical relation, with two adjustable parameters

$$\frac{\Delta R}{R} = \frac{\sqrt{1+4k_n^*\beta^*\langle E\rangle^2}-1}{2k_n^*}, \tag{13}$$

where k_n^* describes the deviation of $\Delta R/R$ from quadratic dependence predicted by (12). Typical values of β^* and k_n^* for n-type Si at a room temperature are collected in Table 1.

Table 1. The parameters β^* and k_n^* for n-type Si at T = 300 K, when the electric field is applied in <111> crystallographic direction.

Specific resistance, Ω·cm	β^*, cm^2/V^2	k_n^*
5	9.0×10^{-8}	3.0
20	9.3×10^{-8}	3.4
200	10.1×10^{-8}	4.3

3.3 Sensitivity

Now we consider a sensitivity of the RS in the linear region where the output signal is proportional to the pulse power P propagating in the waveguide. Since the resistance change of the SE is a quantity indicating pulse power in the waveguide, it is convenient to define the sensitivity of the RS as

$$\zeta = \frac{\Delta R/R}{P}. \tag{14}$$

Definition (14) is not unique. Sometimes the sensitivity is defined as a signal to power ratio. Considering that the signal amplitude depends not only on the DC voltage drop on the RS but on the input resistance of the measurement unit used for the output signal measurement, the proposed definition of the sensitivity is likely more acceptable.

Inserting (12), (10), and (7) into (14) one can get the following expression

$$\zeta = \frac{\beta^*}{\pi a^2}\left[J_0^2(\mu_{11}) + \left(1-\frac{2}{\mu_{11}^2}\right)J_1^2(\mu_{11})\right]^{-1} \frac{\sqrt{\mu_0/\varepsilon_0}}{\sqrt{1-(\lambda/\lambda_c)^2}}\left(\frac{\langle E\rangle}{E_0}\right)^2, \tag{15}$$

describing the sensitivity of the RS in the linear region. It is worthwhile to remind that E_0 in the obtained expression denotes the maximum of the electric field amplitude in the regular H_{11} wave in the center of the empty waveguide. The average electric field is the only unknown quantity in (15). Thus determining it, the sensitivity of the RS in the linear region can be calculated.

Except $\langle E\rangle$ the only multiplier in (15) that influences the dependence of the sensitivity of the RS on frequency is the square root appearing in the denominator of the expression. It indicates the fact that even at the same power level transmitted through the waveguide, the electric field strength in it decreases with frequency because of the wave dispersion in the waveguide. This leads to the decrease of the sensitivity.

Circular waveguides with the H_{11} mode are usually employed in the frequency range λ/λ_c = 0.85–0.6 [5]. From (15) it is easy to get that the sensitivity in this frequency range decreases by a factor of 1.52. If the average electric field in the SE increases by a factor 1.23 in the same frequency range, it will compensate the decrease of the sensitivity due to the wave dispersion in the waveguide and as a result, the RS with flat frequency response will be developed.

Considering this fact and the requirements for the RS formulated in the Introduction, we performed calculations of the average electric field in the SE with a goal to find the RS with the optimal frequency response. When $\langle E \rangle$ is determined, the dependence of $\Delta R/R$ on P can be calculated in a wider dynamical range of the power transmitted through the waveguide. Inserting (10) into (13), one can get the following expression describing the dependence of the relative resistance change on power

$$\frac{\Delta R}{R} = \frac{1}{2k_n^*}\left\{\sqrt{1+\frac{4k_n^*\beta^*}{\pi a^2}\frac{\langle E\rangle^2}{E_0^2}\left[J_0^2(\mu_{11})+\left(1-\frac{2}{\mu_{11}^2}\right)J_1^2(\mu_{11})\right]^{-1}\frac{\sqrt{\mu_0/\varepsilon_0}}{\sqrt{1-(\lambda/\lambda_c)^2}}P}-1\right\}. \qquad (16)$$

3.4 Conclusions

Two configurations of the sensing elements of the RS for the measurement of HPM pulses in the circular waveguide with the H_{11} mode have been considered. Factors influencing the sensitivity of the RS in the circular waveguide were considered, and the requirements for the SE with flat frequency response were formulated.

4 FDTD method

The tremendous increase of the speed and memory of personal computers allows solving three-dimensional electromagnetic problems at a reasonable time. We used the simplest and straightforward finite-difference time-domain (FDTD) method for the calculation of the electromagnetic field components [6, 7] in the structure under investigation. In this section, the model and program used for the calculation of the average electric field in the semiconductor obstacle placed on the wall of the circular waveguide are briefly presented.

4.1 Maxwell's equations

The modeled section of the waveguide with the obstacle is shown in Fig. 5. We used a cylindrical coordinate system and dimensionless coordinates and time: r/a, φ, z/a, $t \cdot v/a$ where

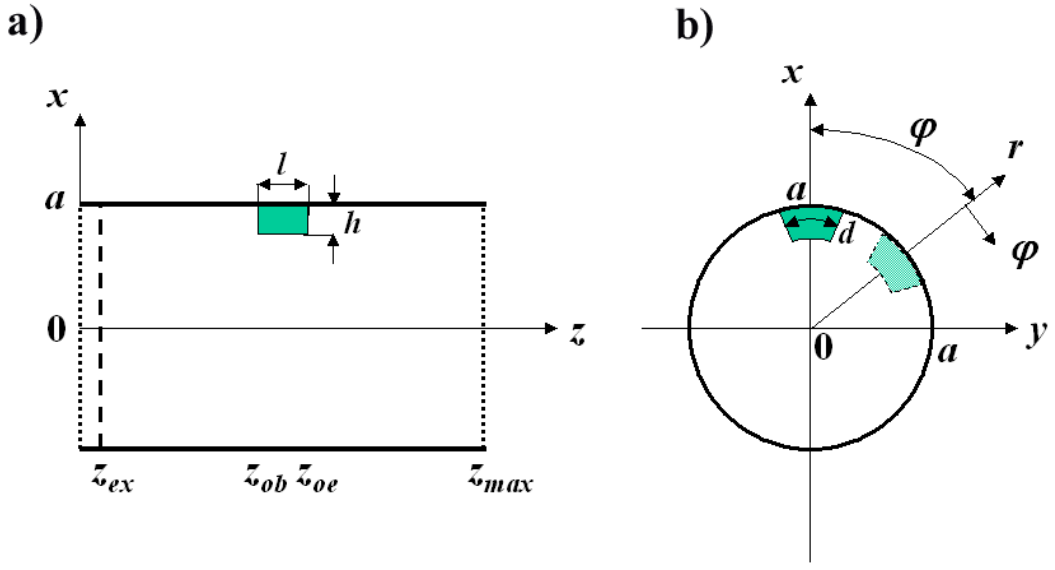

Fig. 5. The sectional view of the modeled circular waveguide with obstacle in $x0z$ plane (a) and $x0y$ plane (b).

v is the velocity of light in free space and a is a radius of the waveguide. In the plane $z=z_{ex}$, the H_{11} type wave is excited. It propagates into both sides from the excitation plane. The obstacle is placed at one wavelength in the waveguide ahead from the excitation plane and at the same distance before the right side of the modeled waveguide section. In the planes $z=0$ and $z=z_{max}$ nonreflecting boundary conditions are satisfied. Therefore, the waves traveling left from the excitation plane as well as reflected from the semiconductor obstacle are absorbed in the plane $z=0$, whereas the wave passing semiconductor structure is absorbed in the plane $z=z_{max}$. Due to the reflection from the semiconductor obstacle the partly standing wave is formed between the planes $z=z_{ex}$ and $z=z_{ob}$. From the amplitude distribution in this area, the reflection coefficient was determined.

The regular H_{11} type wave has five electromagnetic field components (ref. to (1)-(5)). In a vicinity of the SE the E_z component might also appear. Therefore, to determine the average electric field amplitude in the semiconductor obstacle Maxwell's equations have to be solved computing all six components of the electric and magnetic fields. Making use of dimensionless variables and measuring up the magnetic field strength in electric field units Z_0H, where Z_0 is an impedance of free space, Maxwell's equations in the semiconductor obstacle can be written down in a following way

$$\frac{\partial \mathbf{E}}{\partial t} = \left(\nabla \times \mathbf{H} - \gamma \mathbf{E}\right)/\varepsilon, \tag{17}$$

$$\frac{\partial \mathbf{H}}{\partial t} = -\left(\nabla \times \mathbf{E}\right). \tag{18}$$

where $\gamma = Z_0 a/\rho$ accounts for losses in the semiconductor structure. Here ρ and ε are the specific resistance and relative dielectric constant of the semiconductor obstacle, it was assumed that $\mu = 1$ for the entire simulation area. Outside the semiconductor obstacle $\gamma = 0$ and $\varepsilon = 1$. Making use of cylindrical coordinates for the calculation of the curl of the electric and magnetic field and replacing time and coordinate derivatives in (17) and (18) with finite differences, one can obtain the set of equations for updating new values of the components from the older ones. This set can be found in the interim report [3].

The grid of points where the particular component is computed is shifted at a half of step in respect to each other as it was proposed by Yee [6]. Moreover, electric and magnetic fields are calculated at different time moments providing h^2 accuracy in the calculation both space and time derivatives. The details of the application of this technique to the cylindrical coordinate system can be found in monograph [7].

The grid can be chosen in such a way that it starts and finishes with the points where the electric field components should be calculated. Therefore, on the waveguide wall the components E_φ and E_z are zeroed. Depending on the considered configuration of the SE the corresponding components of the electric field are set to zero on the metal contacts: E_φ and E_z for the vertical configuration, E_r and E_z for the horizontal one. In the planes $z=0$ and $z=z_{max}$ nonreflecting boundary conditions for the components E_r and E_φ are satisfied.

At $t \le 0$ there are no electromagnetic fields in the modeled section of the waveguide, therefore all components of the electric and magnetic field are set to zero. When the dimensions of the semiconductor obstacle is much less than the characteristic dimensions of the waveguide its influence on the wave propagating in the waveguide is comparatively small. In such a case, filling the waveguide with the ordinary H_{11} wave components the stationary solution is achieved faster.

Choosing the time step the Courant criterion formulated for 3-D cylindrical coordinate FDTD procedure in [8] was taken into account. Having in mind that the components of the regular H_{11} wave depends on the azimuthal angle φ, in general the average electric field in the SE depends on the angle between the polarization plane and SE. Therefore, the dependence of

the average electric field in the SE on angle φ should be considered as well (Fig. 5b). Let us recall, that the radial component of the electric field of the regular H_{11} wave is at its maximum in the polarization plane $x0z$ (1) while the azimuthal – in the perpendicular plane $y0z$ (2). When the center of the obstacle is placed on x or y-axes the distribution of electromagnetic field amplitudes is symmetrical in respect to $x0z$ or $y0z$ planes and saving computers memory only half of the waveguide window might be modeled.

When one is dealing with FDTD procedure in cylindrical coordinates a numerical singularity is encountered at $r = 0$. To overcome the singularity we have followed a method proposed in [9] that is based on the use of the Cartesian coordinate system in the vicinity of $r = 0$. Since the method was described in details in interim report [3] and it is independent on the mode propagating in the waveguide, we do not consider it here.

4.2 The program

The program computing the electromagnetic field components was written using C++ programming language. It works as follows. During calculations the amplitudes of the particular component of the electromagnetic field at each point of the investigated structure was summed and stored in additional arrays. After each period, the amplitudes of the electric field components are determined and the average value in the SE is calculated. Obtained value is compared with the value calculated one period before. The calculations are terminated when the relative difference between these values had been less than the predetermined value δ. Otherwise, the successive period has been modeled. The number of periods that are necessary to model depends on the obstacle size and specific resistance. For small obstacles, the difference between amplitudes less than 0.01 can be achieved after 3 periods.

As it was already mentioned in the previous section, the electromagnetic field distribution sometimes might be symmetric in azimuthal direction in respect to a plane laying in the middle of the obstacle. In this case, we used programs calculating the electromagnetic field amplitudes in the half of the waveguide. It is worth to mention that computed results have been compared with those obtained using program calculating electromagnetic field components in a whole waveguide and no difference between results has been obtained.

Calculations have been performed for the waveguide with the inner radius $a = 1$ cm. For such a waveguide the critical wavelength for the H_{11} mode is $\lambda_c = 3.41$ cm (6) that corresponds to the cutoff frequency $f_c = 8.78$ GHz. We performed calculations starting from $f_c/f = 0.85$, $f = 10.3$ GHz, towards higher frequencies. Typical dimensionless values of steps used in calculations were $\Delta z = \Delta r = 0.025$, $\Delta\varphi = 1.406°$, $\Delta t = 3\cdot10^{-4}$, the value of the absolute error was set $\delta = 0.01$.

The written program has been tested modeling the obstacle that totally fills the inner gap of the circular waveguide window. Calculated reflection coefficient values have been compared with the analytical solution in Appendix 1.1. We also compared the average electric field calculated in the obstacle using present program with the results obtained using the Cartesian coordinate system. These results are described in subsection 6.4. A good coincidence between results obtained in different ways proves the eligibility of the written program for the calculation of the average electric field and the reflection from the semiconductor obstacle placed on the wall of the circular waveguide.

Since Maxwell's equations are linear, the solution obtained in the circular waveguide with a radius a at a frequency f for the particular size and specific resistance obstacle (h, l, ρ) can be scaled to the other frequency in the waveguide with radius a' by a simple linear transformation

$$h' = h\frac{a'}{a}, \quad l' = l\frac{a'}{a}, \quad \rho' = \rho\frac{a'}{a}, \quad f' = f\frac{a}{a'}, \tag{19}$$

where primed symbols denote a new size, specific resistance and frequency. As it was already mentioned in Subsection 3.2 in the present investigation we do not take into account the dependence of β^* on frequency. This assumption is valid up to and including X-band. Therefore, wishing to compensate the frequency response of the sensitivity at higher frequency bands the decrease of β^* with frequency should be taken into account [10].

4.3 Conclusions

The model of the semiconductor obstacle is considered and the method to solve Maxwell's equations in the cylindrical coordinate system is briefly presented. The performance of the program written for the calculation of the average electric field in the semiconductor obstacle and the reflection coefficient from it is described.

5 Modeling results: Vertical configuration

In this section, the modeling results for the vertical configuration (contacts on top and bottom surfaces Fig. 4a) are presented. In the first subsection, the resonances that occurring in the dielectric SE inserted in the circular waveguide with H_{11} mode and the influence of electrophysical parameters of the SE on the resonance position and amplitude are considered. The dependence of the electric field in the SE on the position of the polarization plane in respect to the SE is described in this subsection as well. The resistive sensor with optimized frequency response is presented in the second subsection. The dependence of the sensitivity on the angle between the SE and polarization plane is considered in the third subsection. The peculiarities of the average electric field in the SE as well as in the whole waveguide section containing a semiconductor obstacle are considered in the fourth subsection.

5.1 Resonances

The large value of the relative dielectric constant of Si $\varepsilon = 11.9$ enforces considerable decrease of the wavelength of the electromagnetic wave in it. Therefore, even in a small dimension obstacles placed in the waveguide some resonances might occur. It was also confirmed by our earlier investigations of the semiconductor obstacles in the rectangular waveguide [10, 11]. In the interim report [3], we have demonstrated that for H_{01} mode the position of the resonance in the frequency scale and its type strongly depends on the configuration of the metal contacts. Although the distribution of electromagnetic field components in H_{11} mode is more complicated, the same peculiarities as for H_{01} mode are characteristic of the insulating obstacle in the waveguide with H_{11} mode. Namely, E_r component is the largest in the vertical configuration SE while E_φ is the largest in the horizontal one. The other components of the electric field in the obstacle are much smaller in comparison with the main in both configurations. Considering the distribution of the largest electric field component within obstacle in the plane $\varphi 0z$ at the resonance conditions, it was found that the distribution is more or less symmetric in respect to the center of the SE in the wave propagating and transverse directions. The resonance in general is observed when either the length of the structure l or width corresponds to the integer number of $\lambda_d/2$, where λ_d is the wavelength of microwaves in the structure. Since the resonance might be used as a tool for the engineering of the output signal dependence on frequency [10, 11] we considered in more detail the influence of electrophysical parameters of the SE (size and specific resistance) to the resonance phenomena in it.

The survey of those investigations for the vertical configuration is collected in Fig. 6 where the dependences of the average electric field in the obstacle on frequency for different size and specific resistance obstacles are presented. The electric field is normalized to the maximum amplitude of the electric field in the centre of the empty waveguide. The center of the SE is located in the polarization plane ($\varphi = 0°$, ref. to Fig. 5b) where the component E_r is at its maximum (1). Initially, we investigated resonances of the dielectric obstacle by changing one of the parameters; say the length l, while the other parameters had been fixed. The dependence of the resonance position on l is shown in Fig. 6a. It is seen that when the length of the SE is growing, the resonance shifts to the lower frequency. It is usual behavior of the resonance since the larger wavelength wave fits the increased length of the obstacle. The dependence of the resonance position on the transverse dimension is shown in Fig. 6b. It is seen that the increase of d also leads to the decrease of the resonance frequency. One can suppose that the increase of the transverse dimension of the obstacle leads to the stronger coupling of it with the wave propagating through the waveguide and this is the reason shifting

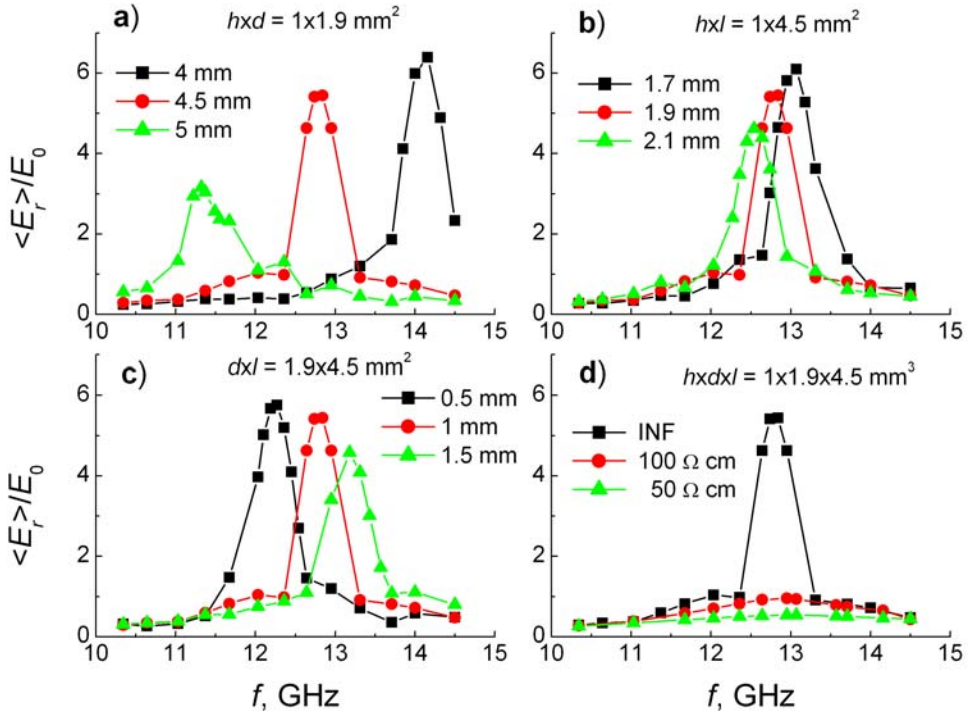

Fig. 6. Calculated dependences of the average of the component E_r in the vertical configuration dielectric obstacle on frequency for the different length l (a), width d (b), and height h (c) obstacles. The dependences of $\langle E_r \rangle$ on frequency for different specific resistance obstacles are shown in subfigure (d). The dimensions of the obstacle and specific resistance (d) of it are specified in the figure. Relative dielectric constant of the obstacle is set 11.9, a = 10 mm.

the resonance to the lower frequency. The results of the calculations for the different height obstacles are shown in Fig. 6c. It is seen that the increase of h leads to the shift of the resonance toward higher frequency. It is worth mentioning that this shift is not so large. Changing the height of the obstacle three times, the resonance is shifted only by 0.9 GHz. In the plane transverse to the axial axis, the obstacle looks as the sector of the ring. While the height of the SE increases, the actual width of it decreases. One might expect that this decrease of the actual width is responsible for the shift of the resonance to the higher frequency. Introduction of losses in the system usually dumps resonance. The SE in the circular waveguide is not the exception. As follows from the results presented in Fig. 6d, electric field strength considerably decreases when the conductivity of the SE increases.

The angular dependence of the resonance in the SE was also investigated since the amplitudes of the electric field in the regular H_{11} wave depends on φ. When $\varphi = 0°$ (ref. to Fig. 5b) the obstacle is mainly exposed by E_r component since $E_\varphi = 0$ (2). At $\varphi = 90°$, on the contrary, the SE is mainly influenced by E_φ since $E_r = 0$ (1).

Calculated dependences of the averaged electric field in the SE on frequency for different φ are shown in Fig. 7. As one can see from the figure, for the strip shape obstacle (Fig. 7a) the position of the resonance is independent of the azimuthal angle. The average electric field component in the SE decreases while the obstacle is shifted towards the y-axis. Considering distribution of the component E_r inside SE in $\varphi 0z$ plane it was found that the $\lambda_d/2$ resonance appears with the maximal electric field at the beginning and end of the obstacle in z direction and minimal electric field in the midpoint of it. It seems that such type of the

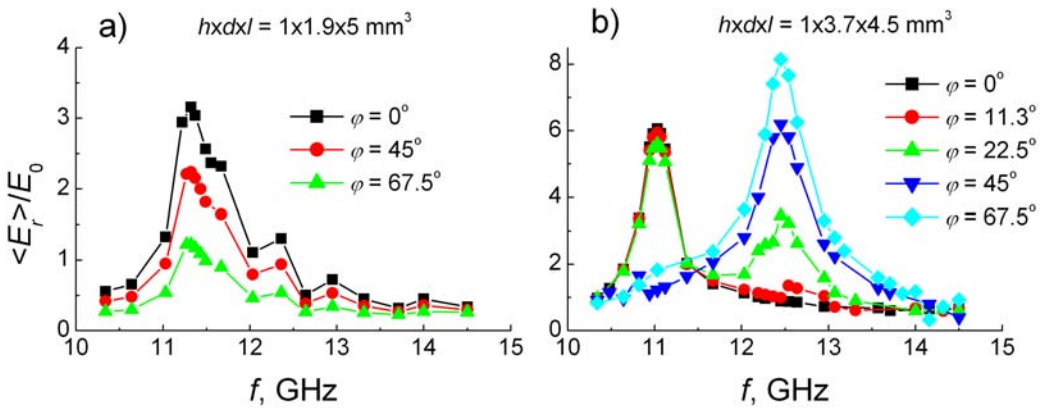

Fig. 7. Calculated dependences of the average of the component E_r in the dielectric obstacle on frequency for the strip shape (a) and plate shape type (b) obstacles located at angle φ from the x-axis. The dimensions of the obstacle and shift angle are specified in the figure. Relative dielectric constant of the obstacle is set 11.9, a = 10 mm.

resonance is tightly connected with the E_r component of the regular wave. Moving the SE towards y-axis the amplitude of the E_r in regular wave decreases causing in turn the decrease of the average electric field amplitude in the obstacle.

The dependences of the $\langle E_r \rangle$ on frequency are more complicated for the plate shape obstacle which dimensions in longitudinal ant transverse direction are comparable. As it is seen from Fig. 7b, at a $\varphi = 0$ the resonance appears at 11.0 GHz. While the obstacle is shifted towards the y-axis, this resonance disappears and a new one emerges at a frequency 12.4 GHz. From the distribution of the electric field component E_r in a $\varphi 0z$ plane of the obstacle shown in Fig. 8, it is seen that the competition between longitudinal and transverse resonances takes place in the plate shape obstacle. When the obstacle is mainly exposed by the component E_r ($\varphi = 0$), the longitudinal resonance occurs. It seems that transverse resonance appears when the obstacle is exposed by the component E_φ. At some intermediate angle, both resonances can be distinguished in the dependence of the $\langle E_r \rangle$ on frequency (Fig. 7b).

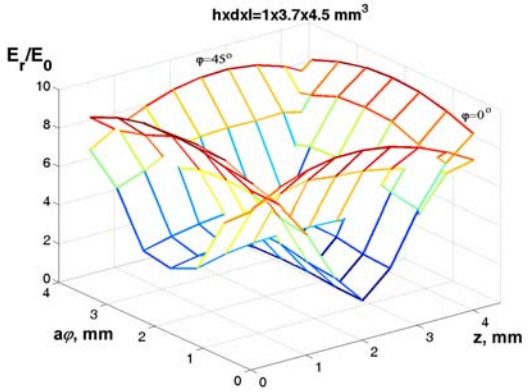

Fig. 8. Distributions in a $\varphi 0z$ plane of the component E_r in the obstacle at a resonance conditions: $\varphi = 0°$, $f = 11.0$ GHz, $\varphi = 45°$, $f = 12.4$ GHz. Dimensions of the obstacle are indicted in the figure.

In conclusion, it may be said that performed investigations revealed the ways to manage the resonance that occurs in the SE placed on the wall of the circular waveguide with H_{11} mode. As in a case of H_{01} mode the position of the resonance in the frequency scale can be easily shifted by changing either the length or the width of the obstacle while the average electric field in it can be adjusted by changing specific resistance of the SE. H_{11} mode is more complicated since the resonance might depend on the position of the SE in respect to the polarization plane. Therefore, in our further investigations for searching the optimal frequency response we shall start from the SE located symmetrically in respect to the polarization plane. Angular dependence of the sensitivity will be considered afterwards.

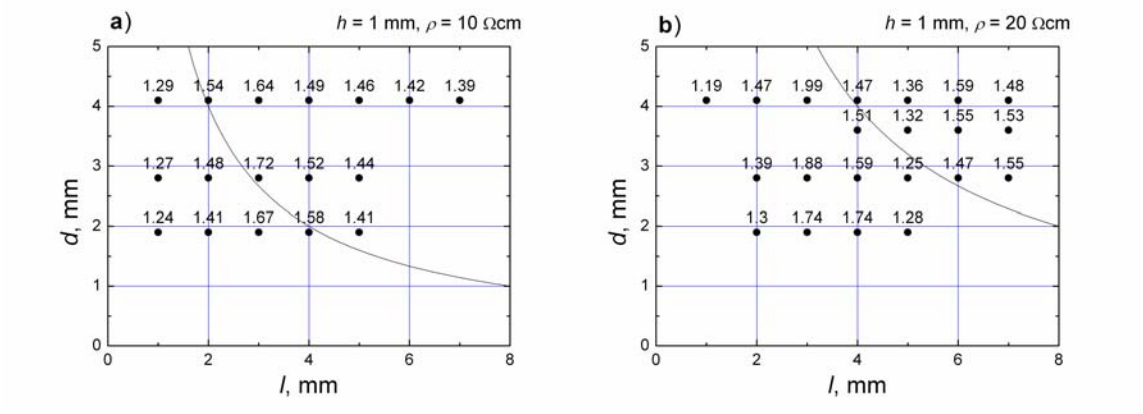

Fig. 9. The ratio of the average electric field of the component E_r calculated at 14.5 GHz to the $\langle E_r \rangle$ calculated at $f = 10.3$ GHz versus longitudinal and transverse dimensions of the SE for $\rho = 10$ Ω·cm (a) and $\rho = 20$ Ω·cm (b). The number near the point corresponds to the value of the ratio for the particular pair of d and l. Waveguide radius is 10 mm, the height of the SE is set 1 mm. The solid curve in the figures corresponds to d and l at which the DC resistance of the RS is 50 Ω. Therefore, above this curve, the resistance of the RS is less than 50 Ω; below this curve, it is more than 50 Ω.

5.2 Frequency response optimization

To optimize the frequency response of the RS, we calculated the dependence of the average electric field $\langle E_r \rangle$ on frequency in the range 10.3-14.5 GHz that corresponds to λ/λ_c = 0.85–0.6. This frequency range has been considered in Subsection 3.3 and it was shown that the increase of $\langle E_r \rangle$ by a factor 1.23 is necessary compensating the decrease of the sensitivity due to wave dispersion in the waveguide. Therefore, our task is to find the values of h, d, l, and ρ at which such increase of $\langle E_r \rangle$ with frequency is observed. As it was already mentioned in the previous subsection initially we investigated the SE placed on the x-axis where E_r is at its maximum.

Taking into account the requirements for the RS formulated in Introduction, we started our search for the set of the optimal electrophysical parameters of the SE considering its height $h = 1$ mm. Such height comprises 1/10 of the radius of the waveguide so one might expect small perturbation of the waveguide by the obstacle. Results of the calculations are shown in Fig. 9. Numbers in the figure near the particular point show a ratio $\langle E_r \rangle$(14.5 GHz)/$\langle E_r \rangle$(10.3 GHz) calculated for the particular pair of d and l. Solid line in the figures corresponds to 50 Ω DC resistance of the RS. Below this curve, the resistance of the RS is larger than 50 Ω, whereas above it $R < 50$ Ω. Considering results shown in the figure, one can see that in general much larger increase of $\langle E_r \rangle$ with frequency is observed than it is necessary to compensate decrease of the electric field in the waveguide due to wave dispersion. Only very short sensors demonstrate the increase of $\langle E_r \rangle$ that is more or less acceptable for the

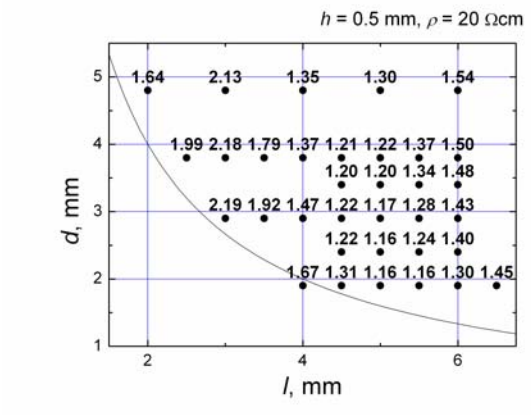

Fig. 10. Dependence of $\langle E_r \rangle$(14.5 GHz)/$\langle E_r \rangle$(10.3 GHz) on longitudinal and transverse dimensions of the SE for $\rho = 20$ Ω·cm, $h = 0.5$ mm, $a = 1$ cm.

compensation of the frequency response, but they resistance is larger than 50 Ω and such a sensor is not suitable for the registration of the short HPM pulses. It should be noted that the situation is not improved by decreasing specific resistance of SE. Calculations for $\rho = 5$ Ω·cm demonstrate practically the same growth of $\langle E_r \rangle$ within considered frequency range. It seems that the SE with $\rho = 20$ Ω·cm and $l = 5$ mm demonstrate the smallest increase of electric field with frequency but it resistance is more than 50 Ω.

The resistance of the sensor decreases by decreasing its the height. Thus, the SE with $h = 0.5$ mm was investigated expecting to get the sensor with desirable increase of the average electric field with frequency and resistance lower than 50 Ω. Calculation results for such SE is shown in Fig. 10. As one can see from the figure, for each width of the obstacle except the widest one (d = 4.9 mm) in the length range 4.5-5.5 mm at least a few points can be found where the calculated ratio of $\langle E_r \rangle$(14.5 GHz)/$\langle E_r \rangle$(10.3 GHz) is close to the desirable value 1.23. Detailed investigations of the frequency response for different width d and length l of the SE were performed. The SE under investigation was located in the polarization plane, hence $\varphi = 0$. The results of calculation are collected in Table 2. In the first column of the table the width of the SE is presented. Calculations for particular d have been performed searching for l that provides minimum sensitivity variation. The length and minimum sensitivity variation are displayed in the second and third columns of the table.

Table 2. The length l of the SE at which calculated sensitivity variation is at its minimum within 10.3–14.5 GHz frequency range for different width d: h =0.5 mm, $\rho = 20$ Ω·cm, a = 1 cm, $\varphi = 0°$.

d, mm	l, mm	$\Delta\zeta/\zeta$, %
1.9	5.5	±7.0
2.4	5.5	±6.0
2.9	5.0	±6.0
3.4	5.0	±4.5
3.8	5.0	±3.5

As one can see from the table, the smallest variation of the sensitivity is characteristic of the SE with dimensions $d = 3.8$ mm and $l = 5.0$ mm. Its DC resistance is roughly 21 Ω. At a moment it is the optimal SE demonstrating the smallest variation of the sensitivity at $\varphi = 0$. The dependence of the sensitivity on frequency calculated with the help of (15) for such RS is shown in Fig. 11a. In the calculation the value of β^* listed in Table 1 was used. As one can see from the figure, flat frequency response is characteristic of the optimal RS. Due to a small height, the optimal sensor does not perturb much the field distribution in the waveguide.

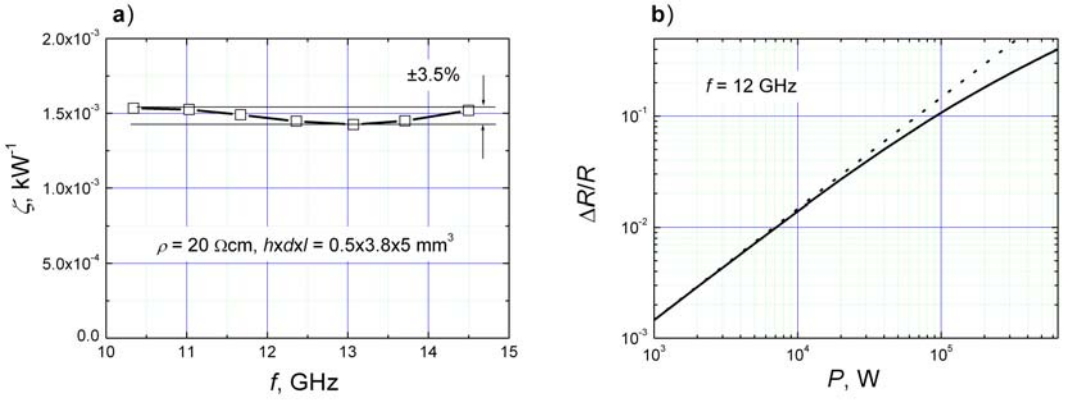

Fig. 11. Calculated dependence of the sensitivity on frequency (a) and dependence of the relative resistance change on power transmitted through the waveguide at $f = 12$ GH for the optimal RS. Solid line in (b) shows results calculated using (16) and dotted line demonstrates linear dependence that is characteristic of the warm electron region. Dimensions of the SE are $h \times d \times l = 0.5 \times 3.8 \times 5$ mm^3, $\rho = 20$ Ω·cm, $a = 10$ mm, $\varphi = 0°$, $R = 21$ Ω.

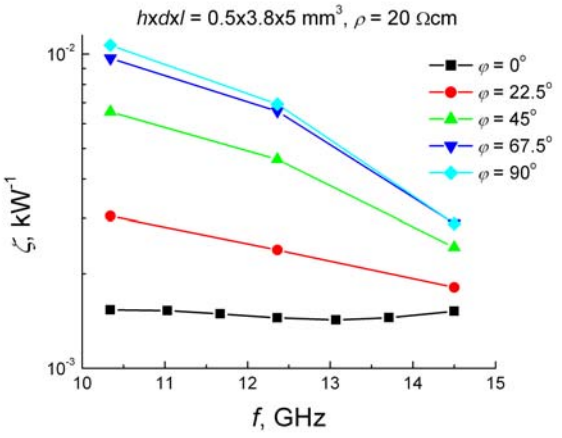

Fig. 12. Dependences of the sensitivity on frequency for the optimal SE at arbitrary position in respect to the polarization plane. An angle between it and the center of the SE is indicated in the figure: $h \times d \times l = 0.5 \times 3.8 \times 5$ mm^3, $\rho = 20$ Ω·cm, $a = 10$ mm, $R = 21$ Ω.

Calculated VSWR slightly increases with frequency, but it is less than 1.03 within considered frequency range.

Once the electric field strength in the SE is determined, the dependence of the relative resistance change on a power transmitted through the waveguide was calculated using expression (16) and parameters of n-Si presented in Table 1. First, we determined maximum power up to which the waveguide with a radius $a = 10$ mm can be potentially used. Considering the electric field strength 25000 V/cm as a limiting due to a breakdown of air, one can calculate the transmitted maximum power P_{max} for the H_{11} mode using expression (10). At $f = 10.3$ GHz 0.65 MW was obtained. As it was already mentioned (Subsection 3.3), at higher frequency more power is required to get the same electric field strength. Therefore, one can consider that the maximum power that can be transmitted through the waveguide ($a = 10$ mm) without breakdown is roughly 0.65 MW and the dependence of the relative resistance change on pulse power transmitted trough the waveguide is calculated using expression (16). Calculation results are shown in Fig. 11b by a solid line. Dotted line corresponds to the linear dependence of $\Delta R/R$ on P that is characteristic of the warm electron region. It is seen that at a maximum power roughly 40% relative resistance change of the SE is observed. It is worthwhile mentioning that the change of resistance in general should influence the average electric field in the SE. Therefore, the curve in Fig. 11b in a high power limit should be considered as some approximation useful to estimate relative resistance change of the RS in the HPM region.

It should be noted, that the optimal RS could be used in the polarization plane only. When the SE is shifted out of plane, its sensitivity becomes dependent on frequency. It illustrates calculation results shown in Fig. 12. It is seen that by shifting the SE from the polarization plane its sensitivity increases. The increase of the sensitivity strongly depends on frequency. Comparing sensitivity at $\varphi = 0°$ and $\varphi = 90°$ it is seen that at a lower frequency the sensitivity increases by a factor 6.5 while in a high frequency range – by 1.9 only. As a result, at a fixed angle φ the considerable decrease of the sensitivity with frequency is observed.

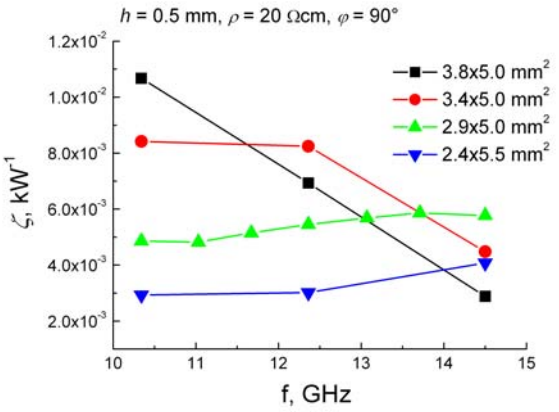

Fig. 13. Dependences of the sensitivity on frequency for the different cross-sectional SE placed at $\varphi = 90°$. Cross-sectional size of the SE is indicated in the figure: $h = 0.5$ mm, $\rho = 20$ Ω·cm, $a = 10$ mm.

Either polarization plane is unknown, or it can be turned off by the accidental deformation of the waveguide [4], the measurement accuracy employing the optimal RS might be poor. One of the

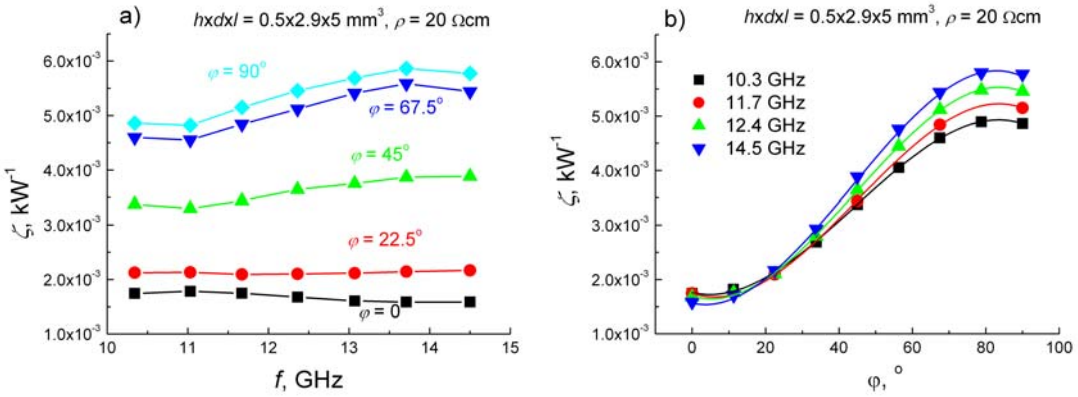

Fig. 14. Calculated dependences of the sensitivity on frequency (a) for several φ and dependences of the sensitivity on φ for several frequencies. The angles and frequencies are indicated in the figure. Solid lines in (b) corresponds to the third order polynomial approximation. Dimensions of the SE are $h \times d \times l = 0.5 \times 2.9 \times 5$ mm^3, $\rho = 20$ Ω·cm, $a = 10$ mm, $R = 28$ Ω.

possible solutions of the problem is the design of the SE that can be rotated in the plane perpendicular to the axial direction. By turning the SE, the position can be found where the output signal is at its minimum. This position corresponds to the polarization plane in the cylindrical waveguide. Therefore using such design polarization plane can be found experimentally. In the next subsection, the other possibility to solve the problem using more than one SE in the waveguide will be considered.

5.3 Angular dependence compensation

Considering angular dependences of the sensitivity of the SE listed in Table 2, it was found that decreasing its width flatness of the sensitivity is improved. It illustrates calculation results shown in Fig. 13 for the SE situated at $\varphi = 90°$ from the polarization plane. As one can see from the figure, a steep decrease of the sensitivity, that is characteristic of the widest SE under investigation, changes to the increase while the width of the SE is reduced. For the further investigation we choose the SE with dimensions $d \times l = 2.9 \times 5$ mm^2 demonstrating the smallest ±10% sensitivity variation within considered frequency range.

We calculated the dependences of the sensitivity on frequency for such size SE for different angle φ between polarization plane and center of the SE. These calculations results are shown in Fig. 14. As one can see from the figure, when the angle φ increases, the sensitivity characteristic becomes overcompensated – electric field strength in the SE increases more than it is necessary to compensate the wave dispersion in the waveguide. The dependences of the sensitivity on the angle

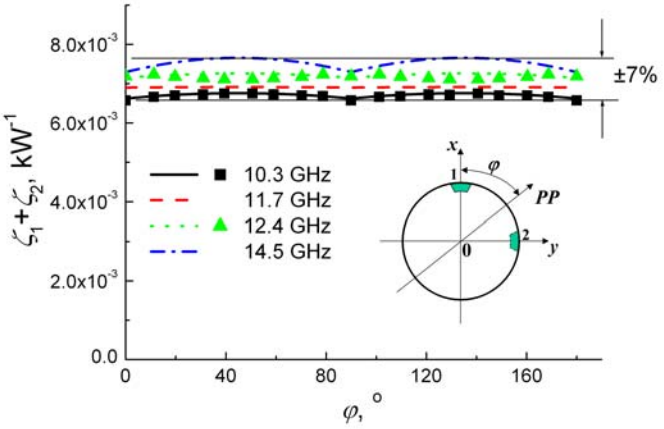

Fig. 15. Dependences of the summed sensitivity of two SE on the angle between one of the SE and polarization plane for several frequencies. Lines correspond to the results obtained using polynomial approximation, points – direct calculation. In the inset, the layout of the sensors in the waveguide is shown schematically. Parameters of the SE: $h \times d \times l = 0.5 \times 2.9 \times 5$ mm^3, $\rho = 20$ Ω·cm, $R = 28$ Ω.

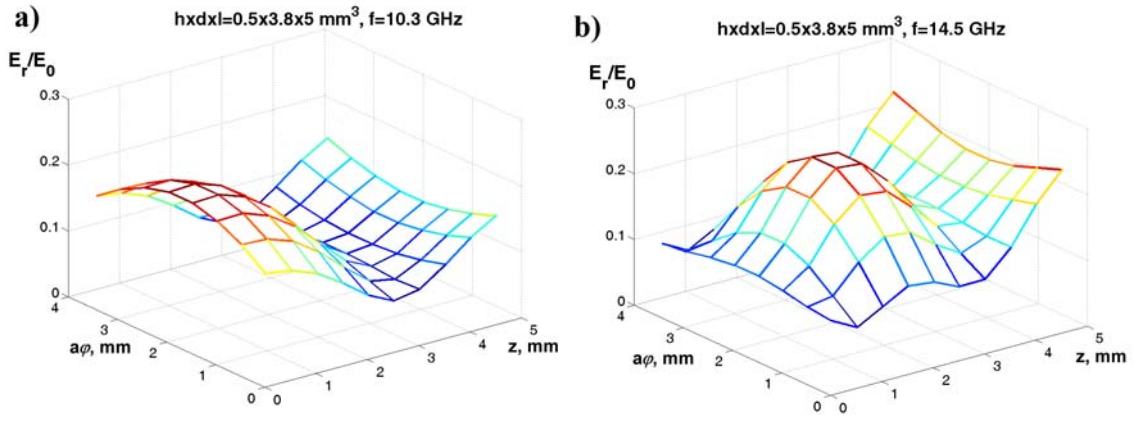

Fig. 16. Calculated distribution of the averaged in r direction electric field component E_r within SE at 10.3 GHz (a) and 14.5 GHz (b). Dimensions and specific resistance of the SE are: $h \times d \times l = 0.5 \times 3.8 \times 5$ mm^3, $\rho = 20$ Ω·cm, it is placed at $\varphi = 0°$, $a = 10$ mm.

between the center of the SE and polarization plane are shown in Fig. 14b. Points in the figure correspond to the calculation results; lines demonstrate approximation of these results by third order polynomial. It is seen that the approximation fits well the calculation results. Considering in more detail the dependences of the sensitivity on φ one can see that they are really symmetric in respect to $\varphi = 45°$. This fact suggests an idea to employ two SE placed at $\varphi = 90°$ in between and, by summing up their signals, compensate the angular dependence of the sensitivity. The idea was examined using analytical expressions of $\zeta(\varphi)$ obtained approximating calculation results by third order polynomial and having in mind that by changing φ in the range 0-90° the sensitivity of the SE number 2 shown in the inset in Fig. 15 will be $\zeta(90°-\varphi)$. Calculated in such a way dependences of the summed sensitivity on φ for several frequencies are shown in Fig. 15 by lines. Results of the direct calculation of two SE in the waveguide are shown in the same figure by points. It is seen that making use of two sensors the angular characteristic of the RS is significantly improved. Calculation shows that using two sensors placed at 90° from each other and measuring the sum of their signals, one can obtain readings independent of the position of the polarization plane in respect to the SE with the accuracy of ±7%. It is worthwhile mentioning that the reflection from two sensors increases negligibly in comparison with single one. Calculated value of the VSWR was less than 1.05 in the considered frequency range.

5.4 Electric field in the sensing element

To have an idea about the electric field strength in the SE the field distribution of the component E_r is shown in Fig. 16 for the SE with the smallest sensitivity variation found. The dimensions of the obstacle are $h \times d \times l = 0.5 \times 3.8 \times 5$ mm^3, its specific resistance $\rho = 20$ Ω·cm, and it is placed at $\varphi = 0°$. E_r component is averaged within obstacle in r direction. It is seen that E_r distribution is symmetric in respect to the azimuthal direction. For the lower frequency, the maximum of electric field is formed at the beginning of the SE and it shifts to the centre when frequency increases. The same dependence is characteristic of the narrower SE used in the two SE configuration. It confirms results shown in Fig. 17a and b where the distribution of E_r at $\varphi = 0°$ is shown. At $\varphi = 45°$, the distribution of E_r in the SE becomes asymmetric forming electric field maximum in the opposite corners of the structure (ref. to Fig. 17c and d). When the SE is situated on y-axis ($\varphi = 90°$), it is seen from Fig. 17e and f that distribution of the component E_r is again symmetric with a minimum in the center of the SE

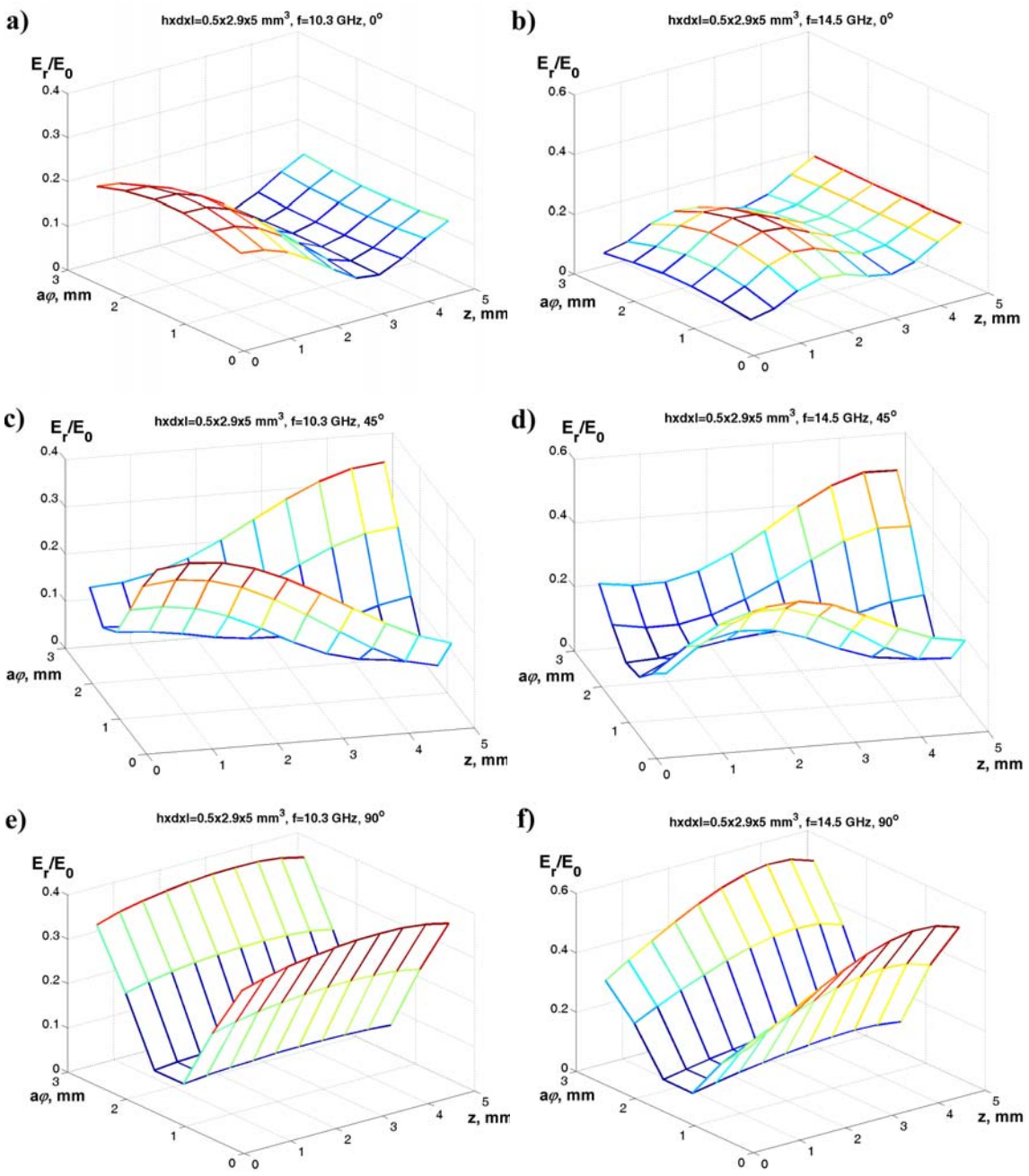

Fig. 17. Calculated distributions of the averaged in r direction electric field component E_r within SE at 10.3 GHz (a),(c),(e) and at 14.5 GHz (b),(d),(f); $\varphi = 0°$ (a),(b), $\varphi = 45°$ (c),(d), $\varphi = 90°$ (e),(f). Dimensions and specific resistance of the SE are: $h \times d \times l = 0.5 \times 2.9 \times 5$ mm^3, $\rho = 20$ Ω·cm, $a = 10$ mm.

in the azymuthal direction. The change of the symmetry in E_r distribution in the obstacle was mentioned in subsection 5.1 considering distribution of the electric field in the dielectric obstacle under resonance conditions.

Electric field in the SE mainly has the E_r component. The other two components E_φ and E_z are much smaller. It illustrates calculation results of components of the average electric field in the SE for 10.3 and 14.5 GHz and several angles of φ shown in Table 3 for the SE with dimensions and specific resistance: $h \times d \times l = 0.5 \times 2.9 \times 5$ mm^3, $\rho = 20$ Ω·cm. As follows from the table, $\langle E_\varphi \rangle$ is roughly 200 times less than $\langle E_r \rangle$ while $\langle E_z \rangle$ is even smaller. It worthwhile mentioning that the increase of h leads to some grow of E_φ and E_z.

Table 3. The average electric field components in the SE for two frequencies and several azimuthal angles φ. Dimensions of the SE $h \times d \times l = 0.5 \times 2.9 \times 5$ mm^2, $\rho = 20$ Ω·cm.

φ, °	10.3 GHz			14.5 GHz		
	$\langle E_r \rangle / E_0$	$\langle E_\varphi \rangle / E_0$	$\langle E_z \rangle / E_0$	$\langle E_r \rangle / E_0$	$\langle E_\varphi \rangle / E_0$	$\langle E_z \rangle / E_0$
0	0.1401	0.0006	0.0004	0.1641	0.0008	0.0006
45	0.1950	0.0010	0.0003	0.2568	0.0013	0.0005
90	0.2339	0.0013	0.0002	0.3131	0.0016	0.0003

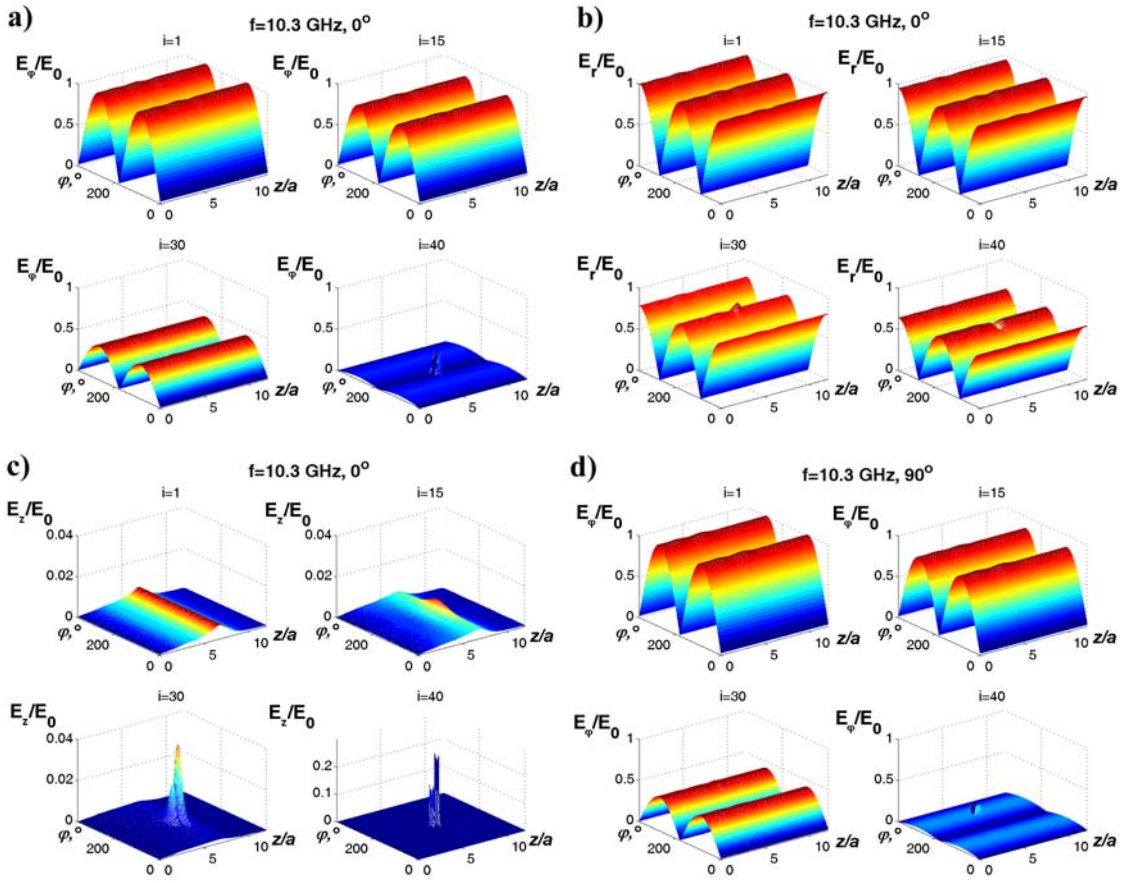

Fig. 18. Distributions of components of the electric field in the waveguide with the SE on the different surfaces $\varphi 0z$ at $f = 10.3$ GHz: E_φ at $\varphi = 0°$ (a) and $\varphi = 90°$ (d) for $r = (i\text{-}1)\Delta r$; E_r at $\varphi = 0°$ (b) for $r = (i\text{-}0.5)\Delta r$; E_z at $\varphi = 0°$ (c) for $r = (i\text{-}0.5)\Delta r$; Calculation parameters: $\Delta r = 0.025$, $\Delta z = 0.05$, $\Delta\varphi = 2.8°$, $\Delta t = 4.50 \cdot 10^{-4}$. Dimensions of the SE are $h \times d \times l = 0.5 \times 2.9 \times 5$ mm^3, $\rho = 20$ Ω·cm, $a = 10$ mm.

Distributions of components of the electric field in the waveguide section with the SE are shown in Fig. 18. Distributions of the components E_φ (a) and (d), E_r (b) and E_z (c) in different $\varphi 0z$ planes are presented. It should be noted that at $\varphi = 0°$ the SE is actually situated at $\varphi = 180°$ and $\varphi = 90°$ corresponds to the angle 270°. Those positions are symmetric in respect to the distribution of the electric field in the regular wave. As it is seen from the figure, due to a small height of the SE, the perturbation of the regular components of H_{11} wave is small except the planes close to the SE. The component E_z that is absent in the regular wave is excited but its amplitude is very small; less than 1% in the center of the waveguide. It becomes more significant in the obstacle or near it. It should be noted that the distribution of

the electric field does not changes much with frequency. Therefore, the distributions only at the lowest considered frequency are shown.

5.5 Conclusions

The resonance occurring in the dielectric obstacle with metal contacts on its top and bottom (vertical configuration) placed in the circular waveguide with regular H_{11} wave was considered. It was found that the resonance position in a frequency scale could be shifted to the lower frequency by increasing the length and width of the obstacle. The average electric field strength in the obstacle can be reduced by increasing its conductivity.

It was established that the average electric field in the SE mainly consists of the E_r component. The components E_φ and E_z are less significant. They increase when the height of the SE grows.

The optimal SE found at a moment should have the following dimensions and specific resistance: $h \times d \times l = 0.5 \times 3.8 \times 5$ mm^3, $\rho = 20$ Ω·cm. It should be placed in the polarization plane of H_{11} wave. Calculated sensitivity variation of the optimal RS was within ±3.5% in the frequency range 10.3–14.5 GHz. The DC resistance of the optimal RS was 21 Ω. Reflection introduced in the waveguide by the RS is sufficiently small: VSWR < 1.03 within frequency range under consideration. The optimal RS can be used for the measurement of HPM pulses propagating in the circular waveguide close to the breakdown in the waveguide.

Since the signal from the optimal RS depends on the position of it in respect to the polarization plane, the SE rotatable in the plane perpendicular to the axial direction has been proposed. The minimum signal from the RS corresponds to the position of the polarization plane in the waveguide.

The alternative RS has been proposed consisting of two SE ($h \times d \times l = 0.5 \times 2.9 \times 5$ mm^3, $\rho = 20$ Ω·cm) placed at 90° from each other. It was shown that the sum of their signals within ±7% is independent of the position of the polarization plane in the waveguide. The DC resistance of each sensor was 28 Ω. Calculated value of the VSWR for two SE was less than 1.05 within the considered frequency range.

6 Modeling results: Horizontal configuration

In this section, the modeling results for the horizontal configuration (contacts on the sidewalls as shown in Fig. 4b) are presented. In the first subsection, the influence of electrophysical parameters of the SE on the resonance position is considered. The influence of specific resistance and dimensions on the frequency response of the RS is considered in the second subsection. The resistive sensor with optimized frequency response is described in the third subsection. In the fourth subsection, the results of modeling of the SE in Cartesian coordinate system are presented.

6.1 Resonances

In the interim report [3] considering the horizontal configuration obstacle (contacts on the sidewalls) in the cylindrical waveguide with H_{01} mode, it was shown that the major electric field component in the SE is E_φ. The same peculiarity is characteristic of the obstacle in the cylindrical waveguide with H_{11} mode. Since the maximum electric field in the SE is found at $\varphi = 90°$ (ref. to Fig. 5b) where E_φ component of the regular wave is at its maximum (2), all further calculations presented here for the horizontal configuration are at $\varphi = 90°$, unless different angle is indicated.

For the obstacle placed at $\varphi = 90°$ dependencies of the resonance position on the electrophysical parameters of it are the same as for the obstacle in the waveguide with H_{01} mode [3]. As usual, the increase of the length leads to the shift of the resonance position to the lower frequency and the increase of the specific conductivity – to the decrease of the electric field strength in the SE. The position of the resonance might also be changed by varying the height of the obstacle. Increase of h leads to the shift of the resonance to the lower frequency while the increase of the width does not influence much the position of the resonance.

We performed additional simulations to elucidate the influence of the position of the polarization plane of the incident wave in respect to the center of the SE on resonance position and amplitude. Results of the simulation are shown in Fig. 19. It is seen that a clear resonance was obtained at 13.1 GHz. The amplitude of the electric field decreases when the polarization plane approaches to the SE. Averaged in the azimuthal direction distribution of the electric field at $\varphi = 90°$ is shown in Fig. 19b. It is seen that the $\lambda_d/2$ resonance in the wave propagation direction is excited in the structure.

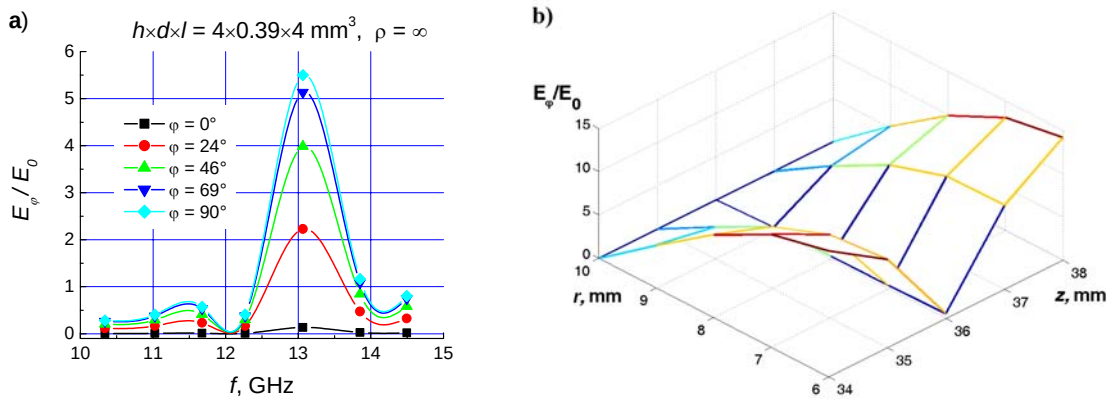

Fig. 19. The average electric field in the dielectric obstacle versus frequency for several polarization angles of the incident wave (a) and the distribution of the electric field averaged in φ direction within the SE at the resonance frequency 13.1 GHz and $\varphi = 90°$. Dimensions of the obstacle are indicated in the figure.

It should be noted that the similar size obstacle was also investigated in vertical configuration (Fig. 7b) and two resonances were discovered. However, in horizontal configuration material of the device is surrounded by three metal interfaces (two contacts plus a wall of the waveguide) instead of two in vertical one. Thus, zero tangential electric field boundary conditions near this third interface do not allow the electric field distribution to be "turned" by 90° that was detected in the vertical configuration (Fig. 8).

Concluding it is worth noting that the position of the resonance in the frequency scale for the horizontal configuration can be easily shifted by changing either the length or the height of the obstacle while the average electric field in it can be adjusted by changing specific resistance of the SE.

6.2 Frequency response optimization

During our investigation, two possible scenarios for optimizing the sensor were considered. First, short sensors were investigated since they shouldn't introduce too much of electric field distortion in the waveguide. By changing the specific resistance of the SE, it should be possible to exploit the interplay between conduction and displacement currents and obtain the desired electric field ratio for different frequencies. Results of these simulations in cylindrical coordinate system are summarized in Fig. 20.

As one can clearly see from the figure, it is possible to obtain electric field ratios close to the desired 1.23, however several practical problems appear. In the case of 20 Ω·cm material (b) it is possible to simultaneously have lower than 50 Ω resistance and the required ratio. However, small change of the dimensions lead to the substantial increase of this ratio, for example, the change of *d* from 0.4 to 0.8 mm leads to an increase of the electric field ratio from 1.29 to 1.54. Therefore, the practical realization of such a sensor could face some difficulties due to unintentional size and positioning variations.

In addition to the investigation of short sensors, we also performed the series of calculations for longer ones at fixed $d = 1.77$ mm and the same fixed height of $h = 2$ mm. These results for both considered specific resistances are also presented in Fig. 20. Unfortunately, only the monotonous decrease of the electric field ratio was obtained for

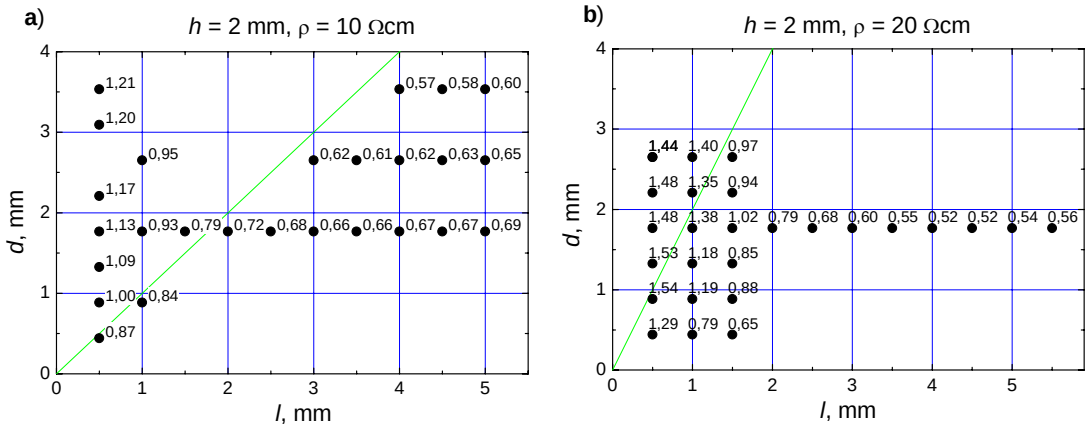

Fig. 20. The ratio of the average electric field $\langle E_\varphi \rangle$ calculated at $f = 14.5$ GHz to $\langle E_\varphi \rangle$ calculated at $f = 10.3$ GHz versus longitudinal and transverse dimensions of the SE for $\rho = 10$ Ωcm (a) and $\rho = 20$ Ωcm (b) material and fixed $h = 2$ mm height. The number near the point corresponds to the value of the ratio for the particular pair of *d* and *l*. The solid curve in the figure corresponds to *d* and *l* at which the DC resistance of the RS is 50 Ω. Therefore, above this curve, the resistance of the RS is more than 50 Ω; below this curve, it is less than 50 Ω. Waveguide radius $a = 10$ mm.

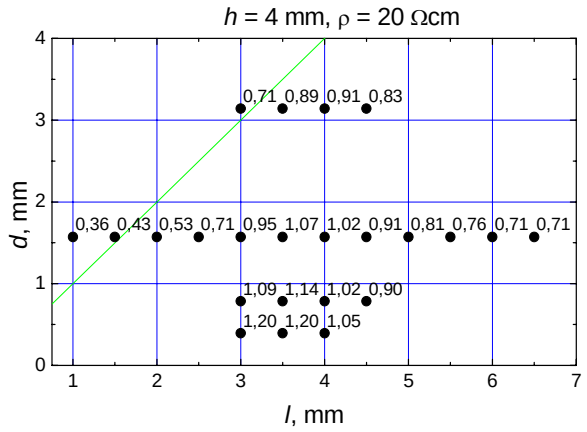

Fig. 21. The ratio $\langle E_\varphi \rangle(14.5)/\langle E_\varphi \rangle(10.3)$ versus longitudinal and transverse dimensions of the SE for $\rho = 20$ Ωcm material and fixed height $h = 4$ mm. The number near the point corresponds to the value of the ratio for the particular pair of d and l. The solid curve in the figure corresponds to d and l at which the DC resistance of the RS is 50 Ω, $a = 10$ mm.

considered specific resistances. Such results indicate that the larger sensors should be investigated due to two reasons: (i) once the length and/or height of the SE is increased the lower resistance is obtained, (ii) the larger size of the SE enhances possibilities to exploit electric field increase near resonant frequencies.

Results of the simulations for "taller" SE are presented in Fig. 21. From the line of ratios corresponding to $d = 1.57$ mm one can clearly see, that the increased height leads to the increase of average electric field ratio once the length of the SE reaches 3 - 4 mm. This is an indication that higher sensors become "massive" enough to have resonant frequencies near the end of the investigated range of frequency and therefore more suitable dependence of the electric field on frequency.

Another favorable feature of this layout becomes noticeable when exploring ratios for fixed l and various d values – electric field at higher frequencies tends to grow faster once the width d is reduced. This feature is particularly important, since reduced width can potentially reduce the reflection coefficient from the sensor. It also should be emphasized, that the electric field ratio changes smoothly once dimensions are changing within 0.5 mm and therefore such a sensor should be more suitable for the reliable production.

6.3 Properties of the optimal sensor

A sensor with dimensions $h \times d \times l = 4 \times 0.4 \times 3.5$ mm^3, $\rho = 20$ Ω·cm, $R = 5.6$ Ω was selected for a more detailed investigation. The calculations were performed at more

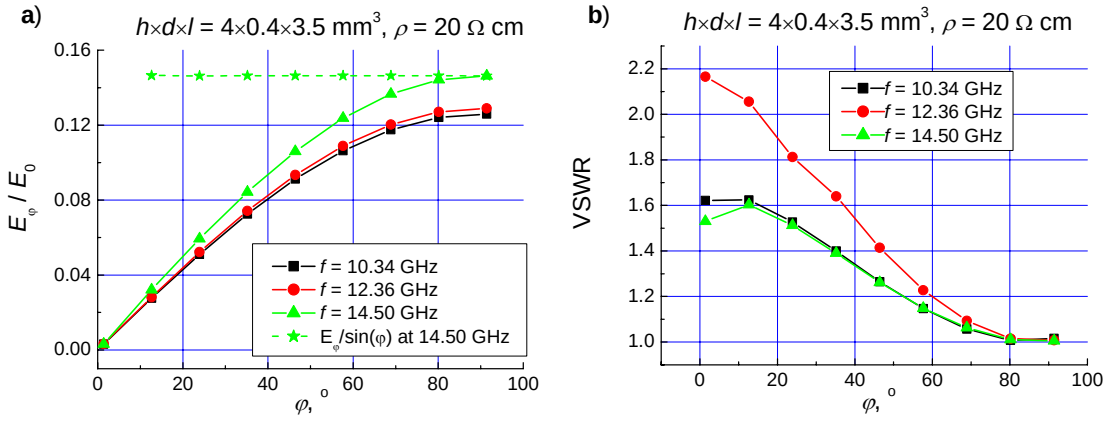

Fig. 22. Dependences of the average electric field within the sensor (a) and VSWR (b) on the angle between center of the SE and polarization plane of the incident wave for several frequencies. The ratio $E_\varphi / \sin\varphi$ is also plotted in (a) for $f = 14.5$ GHz.

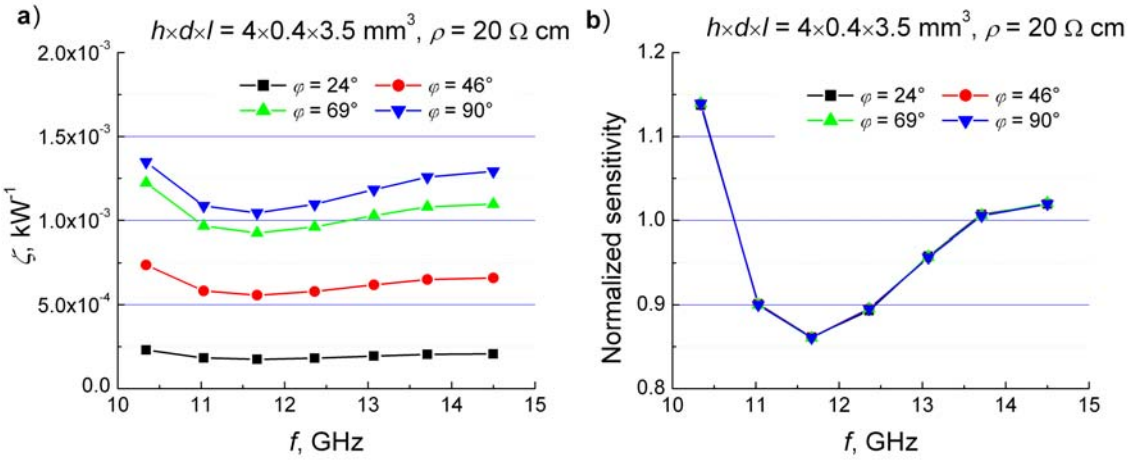

Fig. 23. Dependences of the sensitivity (a) and normalized sensitivity (b) on frequency for the optimal sensor in the horizontal configuration for several different polarization angles indicated in the figure.

frequencies and dependencies on the polarization angle were considered.

Dependencies of the averaged electric field and voltage standing wave ratio on polarization angle for three frequencies are presented in Fig. 22. From Fig. 22a follows that the angular dependence of the average electric field in the SE at 14.5 GHz almost perfectly matches the sin φ dependence that is characteristic of the regular E_φ component of the incident H_{11} wave. It seems that similar angular dependence is typical of the other frequencies as well. Such property can be attributed to the geometry of the SE. It is thin in φ direction and its metal contacts are perpendicular to E_φ electric field component. It is seen that the SE perfectly detects the maximum of the E_φ amplitude ($\varphi = 90°$) at every frequency therefore it means that such device can act as a nearly perfect sensor for the measurement of a local E_φ value. Unfortunately, metal contacts perpendicular to the walls of the waveguide introduce substantial reflections once the SE is placed in the position where E_r value is at its maximum. As follows from Fig. 22b, the VSWR increases substantially for small φ reaching almost the value of 2.2 when the SE is placed in the position $\varphi = 0$.

As in a case of the vertical configuration, the current sensor also should be rotatable, but the maximum of the signal should be found. In such a situation, the SE is perpendicular to the polarization plane of the incident wave. As follows from Fig. 22b, the reflection from the SE can also indicate the desirable position of the SE in respect of polarization plane. At $\varphi = 90°$ VSWR is at its minimum.

An extensive investigation has been performed to reveal more details of the dependence of the sensitivity on frequency. Results of the simulation are presented in Fig. 23. As it can be expected, sensitivity increases with the increase of the angle φ. It was already

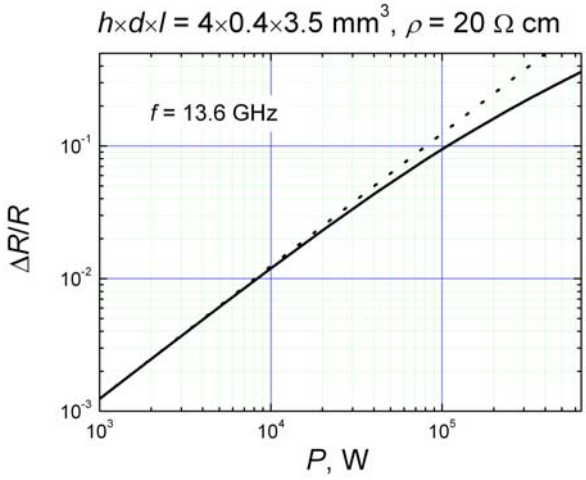

Fig. 24. Calculated dependence of the relative resistance change of the optimal RS on power transmitted through the waveguide at $f = 13.6$ GH. Solid line shows results calculated using (16), dotted line corresponds to linear dependence.

mentioned that the increase of the angle leads to the growth of the component E_φ of the incident wave near the SE. Unfortunately, the absolute value of the sensitivity varies within ±14 % over the entire frequency range. However, normalized sensitivity remains the same within 1.2 % for every fixed frequency, confirming, that this device can be of some use as nearly the ideal sensor for a fixed frequency to determine the position of the polarization plane in the waveguide.

Once the electric field strength in the SE is determined, the dependence of the relative resistance change on a power transmitted through the waveguide can be calculated in the similar manner as in subsection 5.2, Fig. 11b. Calculation results are shown in Fig. 24 by a solid line. Dotted line corresponds to the linear dependence of $\Delta R/R$ on P that is characteristic of the warm electron region. It is seen that at a maximum power roughly 35% relative resistance change of the SE is observed.

Due to a small width of the optimal SE, the averaged electric field in it consists of E_φ component only. The amplitude of the component E_r is roughly 10^{-4} and E_z is even smaller. The distributions of the electric field components in the waveguide section with the SE are shown in Fig. 25. The distribution of the components E_φ (a) and (d), E_r (b) and E_z (c) in different $\varphi 0z$ planes are shown. It is seen that due to a small width of the SE, the perturbation of the regular components of H_{11} wave at $\varphi = 90°$ is small (a and b). VSWR for this particular

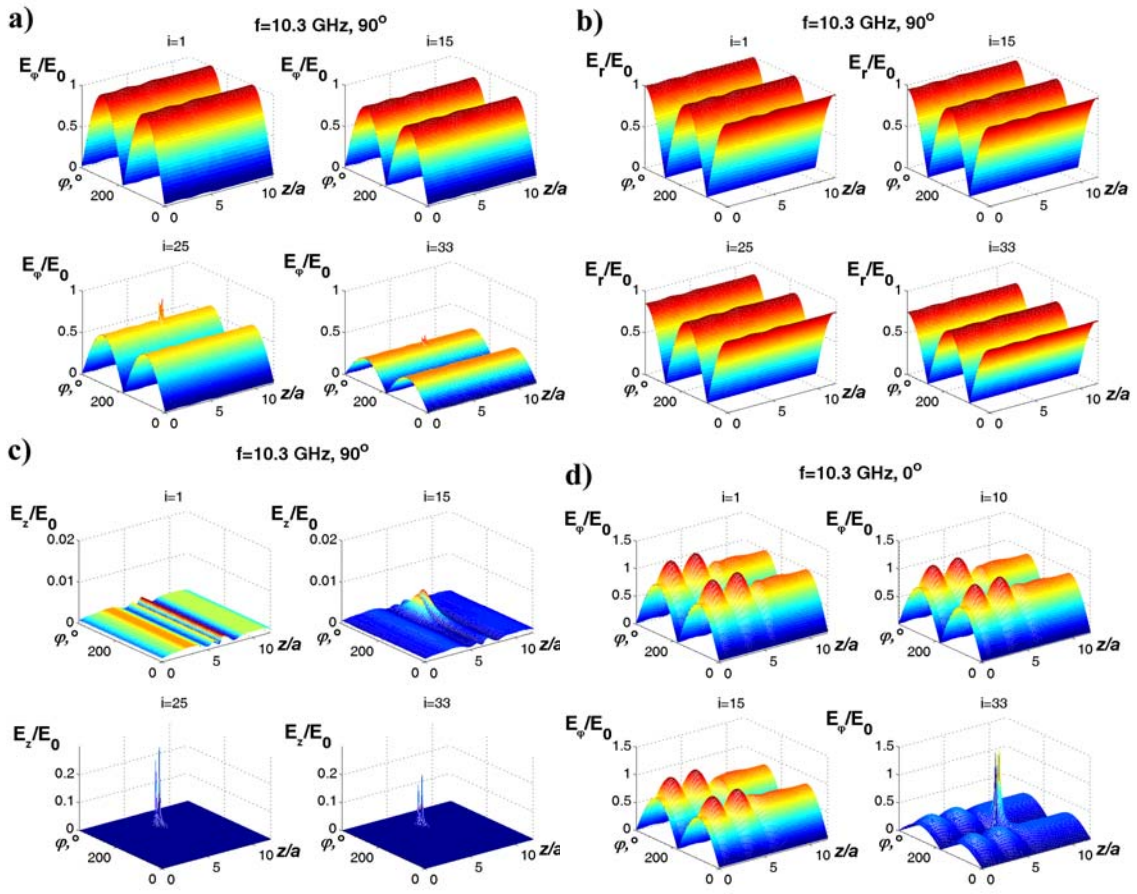

Fig. 25. Distributions of the components of electric field in the waveguide with the SE on the different surfaces $\varphi 0z$ at $f = 10.3$ GHz: E_φ at $\varphi = 90°$ (a) and $\varphi = 0°$ (d) for $r = (i\text{-}1)\Delta r$; E_r at $\varphi = 90°$ (b) for $r = (i\text{-}0.5)\Delta r$; E_z at $\varphi = 90°$ (c) for $r = (i\text{-}0.5)\Delta r$; Calculation parameters: $\Delta r = 0.025$, $\Delta z = 0.05$, $\Delta\varphi = 2.8°$, $\Delta t = 6.10 \cdot 10^{-4}$. Dimensions of the SE are $h \times d \times l = 4.0 \times 0.4 \times 3.55$ mm^3, $\rho = 20$ Ω·cm, $a = 10$ mm.

case is roughly 1.02. Some perturbation of the regular wave is seen in the planes close to the SE. The component E_z that is absent in the regular wave is excited but its amplitude is very small less than 1% in the center of the waveguide. It becomes more significant in the obstacle or near it. The distribution of electric field changes significantly when the position of the SE coincides with polarization plane (d). Partly standing wave between the SE and the excitation plane appears demonstrating strong reflection from the SE. VSWR for this particular case is roughly 1.6.

6.4 Simulations in Cartesian coordinate system

Semiconductor technology usually deals with parallelepiped shaped objects cut from plates with parallel surfaces (Fig. 26a). The SE considered in the cylindrical coordinate system has tapered cross sectional shape (Fig. 26b). Variation of thickness becomes more substantial when the height of the sensor approaches the radius of the waveguide. Wishing to elucidate the influence of the shape to the sensors sensitivity, we performed several FDTD calculations using Cartesian grid and the parallelepiped shaped SE as it is shown in Fig. 26a.

A comparison of the sensitivity of the SE on frequency for two coordinate systems is presented in Fig. 27. As one can clearly see, sensitivities coincide in a high frequency region demonstrating up to 11 % difference in a low frequency region. The obtained discrepancy might be attributed to the difference in shapes.

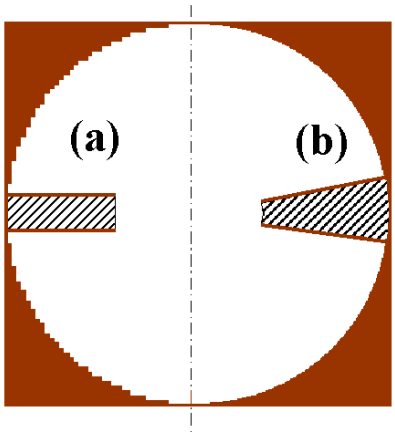

Fig. 26. Sensor's shapes fitting Cartesian (a) and cylindrical (b) coordinates.

6.5 Conclusions

Two possible scenarios for obtaining a nearly flat frequency response of the horizontal configuration sensor (contacts on the sidewalls) were considered. One possibility is to build very short, narrow and relatively high sensor. However, in this case, its resistance is over 50 Ω and its sensitivity is very susceptible to small changes of dimensions. Another possibility is a narrow plate shaped sensor. The optimal SE found at a moment should have the following parameters: $h \times d \times l = 4 \times 0.4 \times 3.5$ mm^3, $\rho = 20$ Ω·cm, R = 5.6 Ω. Such sensor retains the dependence of its normalized sensitivity on frequency for changing the angle between sensor's position and polarization plane of the incident wave, but the sensitivity changes quite substantially ±14 % of the average value in the frequency range 10.3 – 14.5 GHz. Therefore, such sensor would be applicable only for fixed frequency but variable polarization experiments. In general vertical

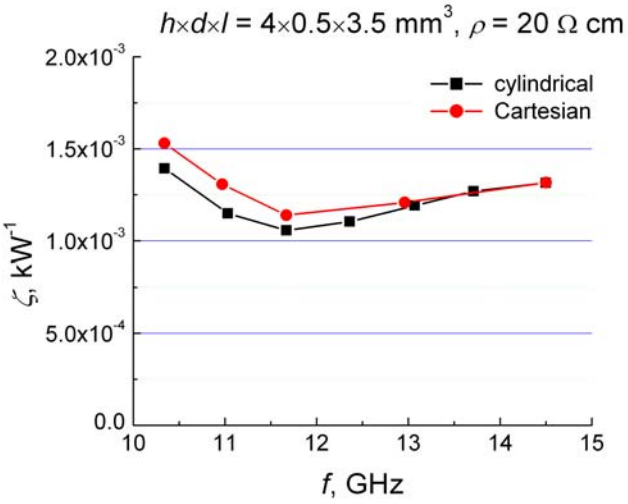

Fig. 27. Dependences of the sensitivity on frequency for the sensor computed in two coordinate systems indicated in the figure.

configuration RS and especially the array of two sensors presented in subsection 5.3 is more preferable.

7 Conclusions

1. Making use of a FDTD method, the peculiarities of the interaction of the semiconductor obstacle placed on a wall of the circular waveguide with a mode H_{11} (TE_{11}) have been investigated. Two different structures have been considered with the contacts on top and bottom planes (vertical configuration) and with the contacts on sidewalls (horizontal configuration). Both these configurations can be considered as a prototypes of the RS devoted for HPM pulse measurement in a circular waveguide.
2. A program based on the FDTD method was written, tested, and used for the calculation of the electromagnetic field components in the circular waveguide with the semiconductor obstacle exposed by H_{11} mode regular wave.
3. Considering the sensitivity of the RS in the circular waveguide, it was shown that the decrease of the sensitivity with frequency occurs due to the wave dispersion in the waveguide. To compensate it the increase of the average electric field in the sensing element of the RS with frequency is required.
4. Considering insulating obstacle in the circular waveguide, it was found that the resonances occur in the structure when the length of the obstacle becomes equal to the integer number of $\lambda_d/2$, where λ_d is the wavelength of microwaves in the structure. In general, the resonance type and frequency depends on the position of the contacts therefore the resonances are different for the vertical and horizontal configurations.
5. The resonance in both configurations can be shifted to the lower frequency by increasing the length of the SE; the averaged electric field amplitude in it decreases when the specific conductivity of the SE grows. For the vertical configuration, the increase of the width of the SE acts on the resonance position in the same way as the length while the change of the height of the SE has little influence on the resonance frequency. For the horizontal configuration, on the contrary, the resonance frequency can be shifted to the lower frequency by increasing its height while the change on the width has little influence on the resonance position.
6. The optimal vertical configuration RS found at a moment should have the following parameters: $\rho/a = 20\ \Omega$, $h/a \times d/a \times l/a = 0.05 \times 0.38 \times 0.5$. Calculated sensitivity variation within frequency range $f_c/f = 0.85–0.60$ for the optimal SE placed in the polarization plane of the incident wave is roughly ±3.5%, where f_c is the cutoff frequency for H_{11} mode. The DC resistance of the RS $R = 21\ \Omega$, calculated VSWR slightly increases with frequency, but it is less than 1.03 within considered frequency range. Since the output signal from the RS depends on its position in respect to the polarization plane, the rotatable SE should be used to find the minimum signal from the RS. In this case, polarization plane coincides with the position of the center of the SE.
7. The alternative RS has been proposed consisting of two SE with parameters: $\rho/a = 20\ \Omega$, $h/a \times d/a \times l/a = 0.05 \times 0.29 \times 0.5$ placed at 90° from each other. It was shown that the sum of their signals within ±7% is independent of the position of the polarization plane in the waveguide. The DC resistance of each RS $R = 24\ \Omega$, calculated value of the VSWR for two SE was less than 1.05 within considered frequency range.
8. The optimal horizontal configuration RS found at a moment should have the following parameters: $\rho/a = 20\ \Omega$, $h/a \times d/a \times l/a = 0.4 \times 0.04 \times 0.35$. Calculated sensitivity variation within frequency range $f_c/f = 0.85–0.6$ for the optimal SE placed in the plane perpendicular to the polarization plane is roughly ±14%. The DC resistance of the RS

R = 5.6 Ω. Since the output signal from the RS depends on its position in respect to the polarization plane, the rotatable SE should be used to find the maximum signal from the RS. In this case, polarization plane is perpendicular to the position of the center of the SE. Calculated VSWR strongly depends on polarization plane position, gaining minimum value at a maximum signal.

9. Comparing optimal sensors found for both configurations, it is seen that both could measure HPM pulse power up to the breakdown in the waveguide. It seems that vertical configuration RS and especially the array of two sensors is more preferable.

8 Acknowledgements

Effort sponsored by the Air Force Office of Scientific Research, Air Force Material Command, USAF, under grant number FA8655-07-1-3028. The U.S. Government is authorized to reproduce and distribute reprints for Governmental purpose notwithstanding any copyright notation thereon.

The views and conclusions contained herein are those of the authors and should not be interpreted as necessarily representing the official policies or endorsements, either expressed or implied, of the Air Force Research Laboratory or the U.S. Government.

9 References

[1] "Fundamentals of RF and microwave measurements," Application Note 64-1a, Hewlett Packard.

[2] M. Dagys, Ž. Kancleris, R. Simniškis, E. Schamiloglu, F.J. Agee, "Resistive Sensor: Device for High-Power Microwave Pulse Measurement", *IEEE Antennas & Propagation Magazine*, vol. 43, No 5, pp. 64-79, 2001.

[3] Interaction Of Semiconductor Obstacle with Electromagnetic Wave Propagating in Circular Waveguide, Interim report, Vilnius, 2007

[4] S. I. Baskakov, *Basics of electrodynamics*, Moscow, Sov. Radio, 1973, (in Russian).

[5] http://www.quinstar.com/qcw_circular_waveguide_sections_and_flanges.html

[6] Kane S. Yee, "Numerical solution of initial boundary value problems involving Maxwell's equation in isotropic media", *IEEE Trans. Antennas Propagation*, 14 (3), pp. 302-307, (1966).

[7] A. Taflove and S.C. Hagness, *Computational Electrodynamics: The Finite-Difference Time-Domain Method*. (Norwood, MA: Artech House 2000).

[8] Q. Chen and V. Fusco, "Three dimensional cylindrical coordinate finite difference time domain analysis of curved slotline", in 2*nd Int. Conf. Computations in Electromag*., U.K., 1994, pp. 323–326.

[9] Ž. Kancleris, "Handling of singularity in finite-difference time-domain procedure for solving Maxwell's equations in cylindrical coordinate system", *IEEE Trans. Antennas Propagation* (accepted).

[10] Ž. Kancleris, V. Tamošiūnas, M. Dagys, R. Simniškis, F. J. Agee, "Interaction of a semiconductor sample partly filling a waveguide's window with millimeter wave radiation", *IEE Proc. Microwaves, Antennas & Propagation*, vol. 152, No 4, pp.240-244, August 2005.

[11] Ž. Kancleris, V. Tamošiūnas, M. Dagys, R. Simniškis, F. J. Agee, "Numerical investigation of resonances within the X-band waveguide type resistive sensors", *IEEE Microwave Wireless Comp. Lett*., vol. 16, pp. 422-424, July 2006.

1 Appendix

Written programs have been tested by comparing computed results with the analytical solution or results obtained using the other programs. In the subsection, the tests are described.

1.1 Comparison with analytical solution

It worthwhile to mention that even small inaccuracies those are left in the FDTD program leads to unstable solution: small inaccuracies are multiplied in the successive steps when the new values of the components of the electromagnetic field are updated from the old ones leading to the infinite growth of them. Therefore, the preliminary testing of the program is very simple. One should get non-infinite values of the electromagnetic field components after a few periods of excitation of the regular wave in the waveguide. The next step that we undertook in program testing was the calculation of the reflection coefficient from the width d dielectric wafer that is tightly inserted into the circular waveguide so that it fully covers its window. From the one hand, the reflection coefficient from such obstacle can be calculated using the program described in Section 4. From the other hand, it can be computed analytically considering plane wave incident at angle θ from the normal to the dielectric plate of width d. For H_{11} mode the wave with **E** in plane of incidence should be considered.

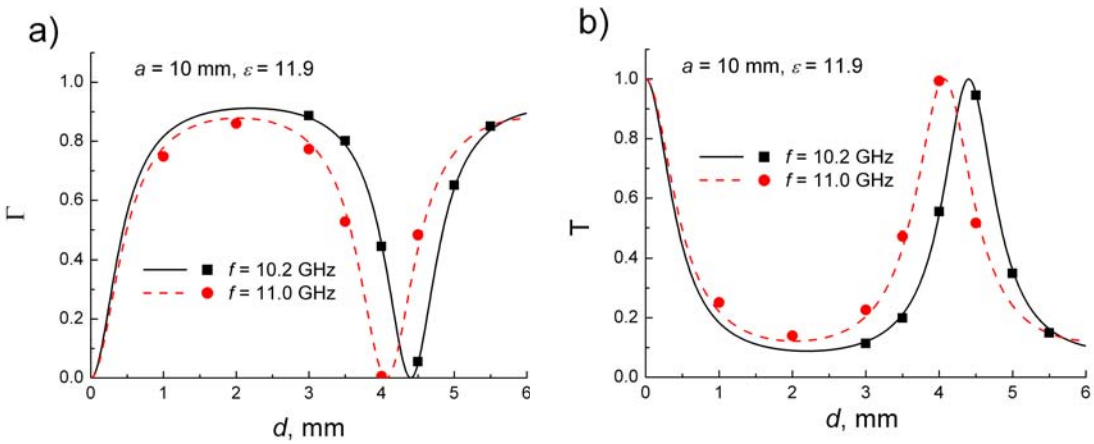

Fig. 28. Dependences of the reflection (a) and transmission coefficients (power) on the width of the dielectric wafer. The wafer is inserted into circular waveguide, mode H_{11}. Lines show analytical solution, points demonstrate calculations results of the FDTD program.

Calculation results obtained using our FDTD program and the analytical solution for two different frequencies are shown in Fig. 28. The radius of the waveguide, the relative dielectric constant and the electromagnetic wave frequency are given in the figure. It is seen that at some thickness of the wafer the Fabri-Perot resonance conditions are fulfilled, the wafer brightens and the reflection coefficient goes to zero. Good coincidence between the numerical results and analytical solution supports the validity of the FDTD program used in the calculations.